

AD-A250 584 ION PAGE

Form Approved  
OMB No. 0704-0188

age 1 hour per response, including the time for reviewing instructions, searching existing data bases, gathering the collection of information. Send comments regarding this burden estimate or any other aspect of this collection of information, including suggestions for reducing the burden, to Washington Headquarters Services, Directorate for Information Operations and Reports, 1215 Jefferson Avenue, Washington, DC 20540, and to the Office of Management and Budget, Paperwork Reduction Project (0704-0188), Washington, DC 20503.

1.

## 3. REPORT TYPE AND DATES COVERED

Annual Technical 4/25/91 - 4/24/92

## 4. TITLE AND SUBTITLE

Femtosecond Studies of Carrier Dynamics in Compound Semiconductors

## 5. FUNDING NUMBERS

N00014-91-J-1956

## 6. AUTHOR(S)

Prof. James Fujimoto

s400067scu01

## 7. PERFORMING ORGANIZATION NAME(S) AND ADDRESS(ES)

Research Laboratory of Electronics  
Massachusetts Institute of Technology  
77 Massachusetts Avenue  
Cambridge, MA 021398. PERFORMING ORGANIZATION  
REPORT NUMBER

## 9. SPONSORING/MONITORING AGENCY NAME(S) AND ADDRESS(ES)

Office of Naval Research  
800 North Quincy Street  
Arlington, VA 22217-500010. SPONSORING/MONITORING  
AGENCY REPORT NUMBER

## 11. SUPPLEMENTARY NOTES

The view, opinions and/or findings contained in this report are those of the author(s) and should not be construed as an official Department of the Army position, policy, or decision, unless so designated by other documentation.

## 12a. DISTRIBUTION/AVAILABILITY STATEMENT

Approved for public release; distribution unlimited.

## 12b. DISTRIBUTION CODE

## 13. ABSTRACT (Maximum 200 words)

Work by Prof. Fujimoto and his collaborators is summarized here.

DTIC  
ELECTE  
MAY 12 1992  
S D D

## 14. SUBJECT TERMS

## 15. NUMBER OF PAGES

## 16. PRICE CODE

17. SECURITY CLASSIFICATION  
OF REPORT

UNCLASSIFIED

18. SECURITY CLASSIFICATION  
OF THIS PAGE

UNCLASSIFIED

19. SECURITY CLASSIFICATION  
OF ABSTRACT

UNCLASSIFIED

## 20. LIMITATION OF ABSTRACT

UL

**Best  
Available  
Copy**

**Progress Report ONR Grant N0001491-J-1956**  
**Femtosecond Studies of Carrier Dynamics in Compound Semiconductors**

April 1992

**James G. Fujimoto**  
Department of Electrical Engineering  
and Computer Science  
Research Laboratory of Electronics  
Massachusetts Institute of Technology

**Christopher J. Stanton**  
Department of Physics  
University of Florida

During the past year we have initiated a new research program to experimentally and theoretically investigate ultrafast processes and carrier dynamics in compound semiconductors. The objective of our program is to apply state of the art femtosecond measurement techniques including high resolution pump-probe absorption spectroscopy and time division interferometry measurements of nonlinear index as well as advanced theoretical techniques including ensemble Monte Carlo calculations and analytic solutions of rate equation models to study transient processes in semiconductors. The combination of experimental and theoretical approaches can be used to provide fundamental information about the physics of excited carriers in semiconductors and how they impact on electronic and optoelectronic device performance.

Experimental efforts at MIT have centered on the development of new techniques for measurement of ultrafast processes in semiconductors and their application to study transient processes in AlGaAs. Studies focus on both femtosecond measurements of nonlinear index as well as absorption. Investigations of nonlinear index are relevant for applications in all optical switching as well as high speed modulation using semiconductor devices. During the past contract year, we have developed a new femtosecond time division interferometry technique for characterizing nonlinear index changes from different components of the  $\chi^{(3)}$  tensor. This new technique uses pump and probe measurements to investigate the amplitude and femtosecond dynamics of the nonlinear phase shift which is induced by a pump pulse on a probe pulse. Because nonlinear index effects are associated with below bandgap excitation, they are extremely small, and sensitive measurements using



waveguide geometries are required. We have developed a new time division multiplexed interferometer scheme which permits the measurement of nonlinear phase shift without parasitic effects from thermal index changes or acoustic vibrations. This new technique permits the characterization of the parallel and perpendicular components of the nonlinear index. Preliminary studies have been performed using optical fibers and semiconductor waveguides. Future investigations will apply this technique to characterize nonlinear index in compound semiconductors as well as quantum confined structures. Future studies will include investigations in the strained layer InGaAs/GaAs systems.

Other ongoing experimental work at MIT focuses on studies of femtosecond carrier dynamics in AlGaAs. We are currently performing pump probe measurements of carrier dynamics in AlGaAs using tunable 40 fs pulses from a high repetition rate femtosecond amplifier. Pump probe absorption saturation measurements are an indicator of the scattering carriers from their initial optically excited states. By varying the wavelength of the excitation pulses, the excess energy of the carrier distributions may be continuously varied. The objective of these studies is to investigate intervalley scattering by varying the carrier energies above and below the allowed energy for scattering from the  $\Gamma$  to the  $L$  valleys.

Finally we are beginning preliminary work on three pulse experiments to investigate the effect of a cold carrier distribution on the relaxation processes of hot carriers. In these measurements an initial electron and hole distribution is prepared by exciting the sample with a variable intensity ultrashort pulse. After a suitable delay to permit the excited characters to thermalize, a standard pump probe measurement is performed. Preliminary measurements have been performed using 2.0 eV pulses of 40 fs duration from a colliding pulse modelocked laser source. Future experiments using tunable pump and probe measurements will permit the investigation of both the scattering of excited carriers with a cold carrier background as well as the effect of high energy carrier excitation on a quasi-equilibrated electron in whole distribution. These experiments have direct bearing on gain and absorption dynamics in laser diodes where perturbations of quasithermal carrier processes produce changes in gain and index in high speed modulation.

Theoretical work at the University of Florida has focused on developing new approaches for studying ultrafast carrier dynamics of carriers photoexcited in GaAs and AlGaAs. Investigations have concentrated on Monte Carlo calculations including both the effects of electron and hole distributions and carrier-carrier scattering as well as analytic rate equation models of pump/continuum probe and tunable pump probe spectroscopy. Because the dynamics of excited carriers in semiconductors is extremely complex, detailed theoretical studies such as ensemble Monte Carlo or rate equation models are required to extract fundamental information on carrier dynamics from experimental measurements. During



Codes	
Dist	Avail and/or Special
A-1	

the past year, we have performed a number of theoretical investigations which are aimed at unifying experiment and theory.

We have developed ensemble Monte Carlo calculational techniques and correlated predicted measurements of pump and probe absorption saturation spectroscopy in GaAs and AlGaAs. These studies resulted in the identification and calculation of Coulomb enhancement effects from excitons near the band edge.

Other Monte Carlo studies have shown the importance of carrier diffusion effects in interpreting the role of carrier dynamics in both semiconductors. Theoretical investigations demonstrated that carrier diffusion can significantly effect the results of pump probe absorption saturation measurements of carrier-carrier scattering on the time scale of 10-100 fs. These investigations demonstrate that differences in sample thickness, even on the scale of 0.2-0.5  $\mu\text{m}$ , affect the interpretation of experimental results by altering the carrier density profiles in the semiconductors.

Finally, we have developed an analytic solution of a rate equation model to describe intervalley scattering. The rate equation approach provides a simpler and computationally less complex model for interpreting femtosecond absorption saturation spectroscopic results. This model has a direct bearing on a number of previous experiments which attempt to measure intervalley scattering rates. Solutions of a rate equation approach show that the return time of electrons from the satellite  $L$  and  $X$  valleys is limited not by the intervalley scattering rate but is instead limited by inelastic scattering within the  $\Gamma$  valley (chiefly through polar optical phonon, POP emission). These results suggest that the accurate measurement of intervalley scattering must depend on the measurement of the initial scattering rate from  $\Gamma$  to  $L$  and not the return rate by which carriers return to the  $\Gamma$  valley.

Future theoretical studies will extend these results and develop a closer correspondence between ensemble Monte Carlo and rate equation models and femtosecond spectroscopic studies. The objective of these investigations is to extract fundamental information on carrier scattering events such as intervalley scattering and role of carrier-carrier scattering including electron hole distributions. Additional studies will extend these results to investigate coherent and non-Markovian processes, i.e., quantum corrections to the standard Boltzmann theory of carrier relaxation, at very short time scales of less than 15 ps.

## 1. PERSONNEL

1. Dr. James G. Fujimoto, Associate Professor of Electrical Engineering, Research Laboratory of Electronics, Department of Electrical Engineering and Computer Science, Massachusetts Institute of Technology, Cambridge, Massachusetts.

2. Dr. Christopher J. Stanton, Assistant Professor of Physics, Department of Physics, University of Florida, Gainesville, Florida.
3. Dr. Lucio Acioli, Visiting Scientist, Massachusetts Institute of Technology.
4. Dr. Daniel W. Bailey, Postdoctoral Associate, (April 1991 - September 1991), University of Florida.
5. Dr. Gary Sanders, Postdoctoral Associate, (October 1991 - present), University of Florida.
6. Morrison Ulman, Research Assistant, Massachusetts Institute of Technology.

## 2. PUBLICATIONS

1. C. de C. Chamon, C. K. Sun, H. A. Haus, and J. G. Fujimoto, "Femtosecond time division interferometry technique for measuring the tensor components of  $\chi^{(3)}$ ," Appl. Phys. Lett. **60**, 533-535, Feb. 1992.
2. L. H. Acioli, M. Ulman, E. P. Ippen, J. G. Fujimoto, H. Kong, B. S. Chen, and M. Cronin-Golomb, "Femtosecond temporal encoding in barium titanate," Opt. Lett. **16**, 1984-1986, Dec. 1991.
3. D. W. Bailey and C. J. Stanton, "Carrier diffusion effects in time-resolved photoluminescence," Appl. Phys. Lett. **60**, 880, 1992.
4. C. J. Stanton and D. W. Bailey, "Rate equations for the study of femtosecond interval scattering in compound semiconductors," Phys. Rev. B **45**, April 1992.

## 3. PAPERS IN PREPARATION

1. C. J. Stanton and D. W. Bailey, "Coulomb enhancement of the above-band edge pump-continuum probe nonlinear absorption," submitted for publication in Physical Review B.
2. D. W. Bailey and C. J. Stanton, "Conduction band anisotropy in GaAs from CW hot electron-acceptor luminescence," submitted for publication in Physical Review B.

#### 4. INVITED TALKS

1. Invited participant, Institute for Theoretical Physics Program on Mesoscopic Physics, Santa Barbara, CA, July 1991.

#### 5. CONTRIBUTED TALKS (MEETINGS)

1. M. Ulman, L. H. Acioli, C. J. Stanton, E. P. Ippen, and J. G. Fujimoto, "Studies of intervalley scattering using tunable femtosecond pulses," to be presented at the Quantum Electronic and Laser Science Conference, QELS'92, Anaheim, CA, May 10-15, 1992.
2. G. D. Sanders, C. J. Stanton, and Y. C. Chang, "Theory of optical gain in silicon quantum wire lasers," presented at the 1992 March Meeting of the American Physical Society, March 16-20, 1992, Indianapolis, IN, paper F19-2.
3. C. J. Stanton and D. W. Bailey, "Rate equations for the study of intervalley scattering in compound semiconductors," presented at the 1992 March Meeting of the American Physical Society, March 16-20, 1992, Indianapolis, IN, paper G20-8.
4. D. W. Bailey, C. J. Stanton, M. Ulman, L. H. Acioli, and J. G. Fujimoto, "Tunable pump-probe nonlinear absorption spectroscopy in AlGaAs," presented at the 1992 March Meeting of the American Physical Society, March 16-20, 1992, Indianapolis, IN, paper G20-7.

# Femtosecond time division interferometry technique for measuring the tensor components of $\chi^{(3)}$

C. de C. Chamon, C. K. Sun,<sup>a)</sup> H. A. Haus, and J. G. Fujimoto  
*Department of Electrical Engineering and Computer Science, Research Laboratory of Electronics,  
 Massachusetts Institute of Technology, Cambridge, Massachusetts 02139*

(Received 3 September 1991; accepted for publication 16 November 1991)

We describe a new femtosecond time division interferometry technique for characterizing nonlinear index changes from different components of the  $\chi^{(3)}$  tensor. Pump probe interferometric measurements of nonlinear phase are performed using a time division multiplexed reference pulse. The  $n_{2\parallel}$  and  $n_{2\perp}$  components of the nonlinear index are measured by permuting the polarizations of the pulses and using a novel differential detection and modulation scheme. Measurements are demonstrated in an optical fiber.

Nonlinear index changes have been investigated using a number of experimental techniques including four-wave mixing,<sup>1</sup> nonlinear waveguide couplers,<sup>2,3</sup> nonlinear Fabry-Perot,<sup>4</sup> fringe shift interferometry,<sup>5</sup> Mach-Zehnder interferometry,<sup>6</sup> and beam propagation distortion.<sup>7</sup> In general, direct measurements of index nonlinearities are complicated because the measurement techniques are sensitive to thermal or acoustical parasitic signals, have low sensitivity, or require deconvolution.<sup>8</sup>

Recently, we have developed a new technique, femtosecond time division interferometry (TDI), that permits high-sensitivity, direct measurements of the nonlinear index  $n_2$  in waveguide devices.<sup>9,10</sup> TDI was previously limited to measurements of  $n_{2\perp}$ , i.e., index changes induced on a probe pulse by an orthogonally polarized pump. However, new materials such as organic polymers, multiple quantum wells and quantum wires are anisotropic and a complete characterization of  $n_2$  requires the measurement of  $n_{2\parallel}$ .

Time-resolved measurements of  $n_{2\parallel}$  are complicated by the fact that both the pump and probe pulses have the same frequency and polarization. In TDI measurements, this degeneracy prevents the interference signal between the probe and reference from being isolated from the interference signals between the pump and probe or the pump and reference. In this letter we report a new extension of the time division interferometry technique that permits measurements of  $n_{2\parallel}$ . The contributions to  $n_2$  from different components of  $\chi^{(3)}$  can be characterized by measuring different permutations of pump and probe polarizations.

The laser source used for our experiments was a mode-locked Nd:YAG which was pulse compressed and frequency doubled to synchronously pump a dye laser. Using the dye Styril 9, the system generates subpicosecond pulses tunable from 795 to 875 nm. The experimental configuration for time division interferometry has been described previously.<sup>9,10</sup> A portion of the laser output is directed to a micrometer-stage delay line to function as the pump. The pump beam is chopped and the phase delay of the pulse is modulated using a PZT attached to one of the delay mirrors. The probe and reference are obtained using a Mich-

elson-type delay line with waveplates and a polarizing beam splitter. This system functions as a polarization sensitive delay line and generates orthogonally polarized probe and reference pulses. Half-wave plates placed in the probe, reference, and pump beams are used to set different combinations of polarizations for the three pulses. The pulses are then coupled into the waveguide structure to be characterized. After the waveguide, the signals are detected using a polarizer and dual detector. Finally, the phase bias operating point of the interferometer is actively stabilized using a PZT on the polarization-sensitive delay line. The feedback error signal is obtained using a boxcar integrator which detects the interferometer output signal when the pump pulse is blocked.

Figure 1 shows the relative positioning of the pulses for the measuring  $n_{2\parallel}$  and  $n_{2\perp}$ . The field amplitudes of the pump, probe, and reference pulses are denoted  $E_{pu}$ ,  $E_{pr}$ , and  $E_{ref}$ . The pump pulse induces a nonlinear phase shift on the probe which is then measured by interfering the probe pulse with a time division multiplexed reference pulse. The reference pulse is then time delayed using a polarization-sensitive delay line so that it interferes with the probe pulse. For the measurement of  $n_{2\parallel}$  the pump pulse does not have a different polarization and thus is not separated from the probe and reference pulses. The phase of the interferometer can be biased by adjusting the polarization-sensitive delay line with a PZT. The nonlinear index is characterized by measuring the phase shift of the probe relative to the reference using a polarizer and differential detector geometry. Finally, the dynamics of the nonlinear index may be measured by varying the delay between the pump and probe pulses.

The details of the measurement technique for  $n_{2\parallel}$  and  $n_{2\perp}$  can be described by performing a simple analysis of the signals which are detected. Let us first consider the case where the pump and probe are perpendicularly polarized. The signals projected along the two polarization axes of the detectors are

$$S_{1,2} \sim |E_{pr}e^{i\phi_{nl}} \pm E_{ref}e^{i\phi_{bias}}|^2 + |E_{pu}|^2, \quad (1)$$

where  $\phi_{nl}$  is the nonlinear phase shift produced by the pump on the probe, and  $\phi_{bias}$  is the bias phase of the interferometer. In order to simplify the equations, we express the field amplitudes as real variables with relative phases expressed explicitly. The square of the field amplitude is

<sup>a)</sup> Present address: Division of Applied Science, Harvard University, Cambridge, MA.



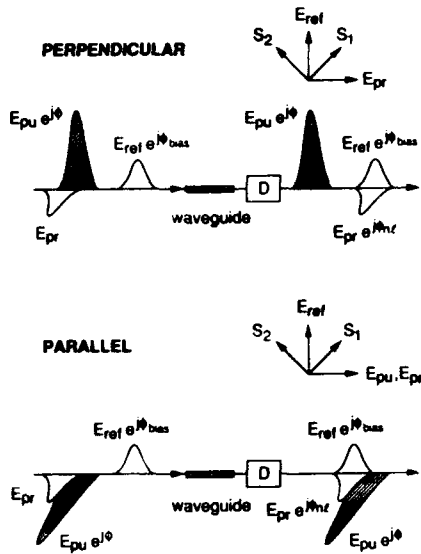


FIG. 1. Relative positioning of the pump, probe, and reference pulses before and after the waveguide sample for measurements of  $n_{2\perp}$  and  $n_{2\parallel}$ . The polarization sensitive delay line,  $D$ , separates pump and probe in the case of the perpendicular measurement, but not in the parallel case.

normalized to intensity. Performing differential detection cancels the background intensity from probe and reference fields and yields the interference term:

$$S \sim 4E_{pr}E_{ref} \cos(\phi_{nl} - \phi_{bias}). \quad (2)$$

For measurements of nonlinear phase, the interferometer is biased to  $\phi_{bias} = \pi/2$ , and the phase changes  $\phi_{nl}$  are small so the signal is given by

$$S \sim 4E_{pr}E_{ref} \sin \phi_{nl} \sim 4E_{pr}E_{ref}\phi_{nl}. \quad (3)$$

Since the pump beam is chopped and  $\phi_{nl}$  is modulated, lock-in amplification detects only the terms that contain  $E_{pu}$ . The contribution of these terms to the nonlinear phase shift is

$$\phi_{nl} = \left( \frac{2\pi}{\lambda} \right) n_{2\perp} E_{pu}^2 E_{ref} \left( 1 + \cos 2\phi \frac{\chi_{1212}^{(3)}(\omega; \omega, -\omega, \omega)}{2\chi_{1221}(\omega; \omega, -\omega, \omega)} \right), \quad (4)$$

where  $\phi$  is the phase between pump and probe and  $n_{2\perp}$  is defined as the Kerr coefficient for monochromatic orthogonal polarizations with the coherence term suppressed. The term containing  $\cos 2\phi$  is the result of cross-phase modulation between the pump and reference. This term is averaged to zero when the pump phase is dithered using a PZT, or when the pump time delay is scanned. The resulting signal permits a measurement of  $n_{2\perp}$ .

$$S \sim 4E_{pr}E_{ref}E_{pu}^2 (2\pi/\lambda) n_{2\perp} L_{eff}. \quad (5)$$

Next let us consider the case where the pump and probe are polarized parallel to each other and interfere. For this case the detected signals in the two polarizations are

$$S_{1,2} \sim |(E_{pr} + E_{pu}e^{i\phi})e^{i\phi_{nl}} \pm E_{ref}e^{i\phi_{bias}}|^2, \quad (6)$$

where  $\phi$  is the phase difference between probe and pump. Differential detection yields

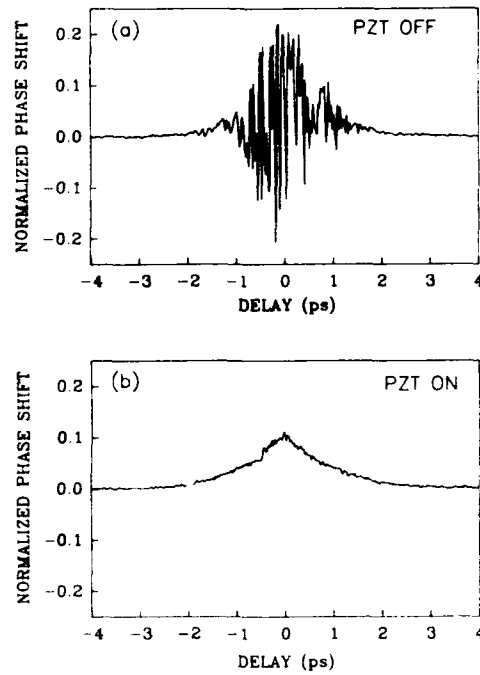


FIG. 2. Time division interferometer measurement performed with and without dithering the phase of the pump pulse.

$$S \sim 4E_{pr}E_{ref} \cos(\phi_{nl} - \phi_{bias}) + 4E_{pu}E_{ref} \cos(\phi + \phi_{nl} - \phi_{bias}). \quad (7)$$

Biasing at  $\phi_{bias} = \pi/2$  for small  $\phi_{nl}$  the detected signal is

$$S \sim 4E_{pr}E_{ref} \sin \phi_{nl} + 4E_{pu}E_{ref} \sin(\phi + \phi_{nl}) \sim 4E_{pr}E_{ref}\phi_{nl} + 4E_{pu}E_{ref}(\sin \phi + \phi_{nl} \cos \phi). \quad (8)$$

The second term in (7) and (8) arises from interference between the pump and reference pulses.

The nonlinear phase shift produced by the pump on the probe is

$$\phi_{nl} = (2\pi/\lambda) n_{2\parallel} (E_{pr}^2 + E_{pu}^2 + 2E_{pr}E_{pu} \cos \phi) L_{eff}, \quad (9)$$

where  $n_{2\parallel}$  is the Kerr coefficient for a monochromatic linearly polarized wave. The third term in (9) is the interference of the pump and probe fields.

In order to suppress the phase-sensitive cross terms and perform a measurement of  $n_{2\parallel}$ , the delay of the pump pulse is dithered by an integer multiple of the wavelength. This averages the terms containing  $\sin \phi$  and  $\cos \phi$  to zero and the term containing  $\cos^2 \phi$  to  $1/2$ . Since lock-in detection is used, the chopping frequency of the pump must be lower than the frequency of the pump phase to average the phase-sensitive contributions in the detected signal. After lock-in amplification the detected signal is

$$S \sim 8E_{pr}E_{ref}E_{pu}^2 (2\pi/\lambda) n_{2\parallel} L_{eff}. \quad (10)$$

Note that the detected signal for the parallel case has exactly the same form as in the perpendicular case except for an extra factor of 2.

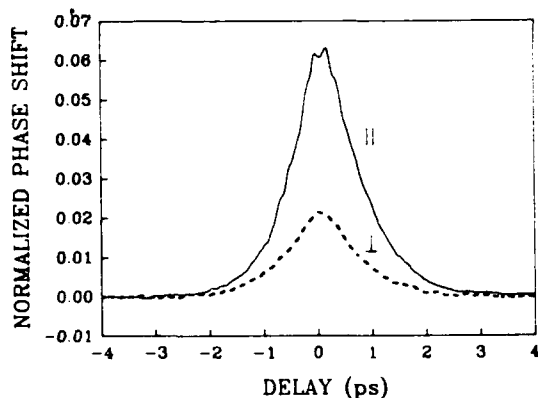


FIG. 3. Time division interferometer measurement of the nonlinear index in an optical fiber for parallel and perpendicular pump and probe. The ratio of the two peaks is  $\sim 3:1$ .

In order to confirm that the measurement technique functions as predicted, experimental studies were performed using an optical fiber. The optical fiber is an isotropic material with well-established nonlinear optical properties. The sample consisted of 83 cm of Corning non-polarization conserving fiber with a 5- $\mu\text{m}$  core diameter. Special care was required in handling and mounting the fiber to avoid stress-induced birefringence effects.

In order to demonstrate the effect of pump phase, measurements were performed using parallel polarized pump and probe pulses, with and without dithering the pump phase  $\phi$  (Fig. 2). Figure 3 shows the experimentally measured phase shift for the parallel and perpendicular pump and probe polarization configurations. The two measurements were performed by rotating the pump pulse polarization  $90^\circ$ . All other parameters, such as the probe and reference pulse polarization, the phase bias,  $\phi_{\text{bias}}$ , and the intensities of all pulses were kept fixed. The pulse duration was 850 fs and the pump pulse energy was 5.5 pJ. Traces were averaged over several scans of the pump pulse delay with a data acquisition time of 2 min.

The ratio  $n_{\parallel}/n_{\perp}$  can be determined from the two curves. From (1) and (2), the ratio between the peaks of the two curves equals  $2n_{\parallel}/n_{\perp}$ . The measured ratio is  $3.00 \pm 0.07$ , which implies  $n_{\parallel}/n_{\perp} = 1.50 \pm 0.04$ . This is in agreement with theoretical predictions based on symmetry considerations. For an isotropic medium,<sup>11</sup>

$$\chi_{1111}^{(3)}(\omega:\omega, -\omega, \omega) = \chi_{1212}^{(3)}(\omega:\omega, -\omega, \omega) + \chi_{1221}^{(3)}(\omega:\omega, -\omega, \omega) + \chi_{1122}^{(3)}(\omega:\omega, -\omega, \omega). \quad (11)$$

In silica fibers the dominant contribution to the nonlinear index is electronic and the three terms on the right-hand side of (11) are approximately equal.<sup>12,13</sup> The contribution from  $\chi_{1212}^{(3)}$  yields a coherent interaction between the pump and probe pulses that averages to zero when the pump phase is dithered. Therefore,

$$\frac{n_{\parallel}}{n_{\perp}} = \frac{\chi_{1111}^{(3)}(\omega:\omega, -\omega, \omega)}{2\chi_{1221}^{(3)}(\omega:\omega, -\omega, \omega)} = \frac{3}{2}. \quad (12)$$

The experiments agree with theory and yield the correct ratio for the two components of  $n_2$ .

The experimental value for  $n_2$  can be obtained from the measured phase shift. In an experiment, the detected signal is averaged over the pulse shape and the transverse area of the waveguide. The measured peak of the detected signal is

$$S = \frac{\int dt \int dA 8E_{\text{pr}}E_{\text{ref}}E_{\text{pu}}^2 (2\pi/\lambda)n_{2\parallel}L_{\text{eff}}}{\int dt \int dA 4E_{\text{pr}}E_{\text{ref}}}. \quad (13)$$

The detected signal is normalized to the output of the interferometer when  $\phi_{\text{bias}} = 0$  and  $E_{\text{pu}} = 0$ .

If the spatial field distribution in the fiber is approximated by a Gaussian,<sup>14</sup> and the temporal profile is also assumed to be Gaussian:

$$S = \frac{2\pi(2n_{2\parallel})L_{\text{eff}}\mathcal{E}\sqrt{2\ln 2/\pi}}{\lambda\tau w^2\pi}, \quad (14)$$

where  $\mathcal{E}$  is the pulse energy,  $\tau$  the pulse FWHM, and  $w$  the field radius (3  $\mu\text{m}$  for the fiber used). Using the results of Fig. 3, the measured value for  $n_{2\parallel}$  is  $3.31 \pm 0.83 \times 10^{-16} \text{ cm}^2/\text{W}$ . This is in close agreement with previous measurements of  $3.2 \times 10^{-16} \text{ cm}^2/\text{W}$ .<sup>15</sup> Finally, it should be noted that the measurement technique is extremely sensitive. The signal-to-noise ratio in Fig. 3 is greater than 10. Thus, phase shifts as small as 5 mrad can easily be detected.

The authors would like to thank Kristin Rauschenbach for helpful scientific discussions. This work was supported in part by the Air Force Office of Scientific Research Contract No. F49620-88-C-0089, the Office of Naval Research Contract No. N00014-91-J-1956, the Joint Services Electronics Program Contract No. DAAL03-89-C-0001, and the National Science Foundation Presidential Young Investigator Award Grant No. ECS-85-52701.

<sup>1</sup>W. K. Burns and N. Bloembergen, Phys. Rev. B **4**, 3437 (1971).

<sup>2</sup>P. Li Kam Wa, J. E. Sitch, N. J. Mason, J. S. Roberts, and P. N. Robson, Electron. Lett. **21**, 27 (1985).

<sup>3</sup>R. Jin, C. L. Chuang, H. M. Gibbs, S. W. Koch, J. N. Polky, and G. A. Pubanz, Appl. Phys. Lett. **53**, 1791 (1986).

<sup>4</sup>Y. H. Lee, A. Charvez-Pirson, S. W. Koch, H. M. Gibbs, S. H. Park, J. Morhange, A. Jeffrey, N. Peyghambarian, L. Banyai, A. C. Gossard, and W. Wiegmann, Phys. Rev. Lett. **57**, 2446 (1986).

<sup>5</sup>G. R. Olbright and N. Peyghambarian, Appl. Phys. Lett. **48**, 1184 (1986).

<sup>6</sup>D. Cotter, C. N. Ironside, B. J. Ainslie, and H. P. Girdlestone, Opt. Lett. **14**, 317 (1989).

<sup>7</sup>M. Sheik-Bahae, A. A. Said, and E. W. Van Stryland, Opt. Lett. **14**, 955 (1989).

<sup>8</sup>M. C. Gabriel, H. A. Haus, and E. P. Ippen, J. Lightwave Technol. **4**, 1482 (1986).

<sup>9</sup>M. J. LaGasse, K. K. Anderson, H. A. Haus, and J. G. Fujimoto, Appl. Phys. Lett. **54**, 2068 (1989).

<sup>10</sup>M. J. LaGasse, K. K. Anderson, H. A. Haus, and J. G. Fujimoto, Appl. Phys. Lett. **56**, 417 (1990).

<sup>11</sup>Y. R. Shen, *The Principles of Nonlinear Optics* (Wiley, New York, 1984), Chap. 2.

<sup>12</sup>Y. R. Shen, *The Principles of Nonlinear Optics* (Wiley, New York, 1984), Chap. 16.

<sup>13</sup>H. A. Haus, "Derivation of instantaneous third order polarizability," Quantum Electronics and Femtosecond Optics Memo. No. 13 (MIT Research Laboratory of Electronics, Cambridge, MA, 1987).

<sup>14</sup>D. Marcuse, J. Opt. Soc. Am. **68**, 103 (1978).

<sup>15</sup>R. H. Stolen and C. Lin, Phys. Rev. Lett. **17**, 1448 (1978).

# Femtosecond temporal encoding in barium titanate

L. H. Acioli,\* M. Ulman, E. P. Ippen, and J. G. Fujimoto

Department of Electrical Engineering and Computer Science, Research Laboratory of Electronics,  
Massachusetts Institute of Technology, Cambridge, Massachusetts 02139

H. Kong, B. S. Chen, and M. Cronin-Golomb

Electro-Optics Technology Center, Tufts University, Medford, Massachusetts 02155

Received September 30, 1991

We describe two-beam coupling and temporal encoding experiments in barium titanate. Volume gratings are created in the photorefractive material by 50-fs optical pulses. Information in the writing pulses may be encoded as spatially distributed volume gratings in the crystal. Femtosecond temporal waveform reconstruction is demonstrated.

The nonlinear-optical properties of photorefractive materials have been extensively studied in wave-mixing experiments, most of which have been conducted using cw lasers as light sources.<sup>1</sup> Recently picosecond pulsed lasers with low and high repetition rates have also been used for the study of photorefractive materials<sup>2,3</sup> as well as for coherence time measurements of the incident fields.<sup>4,5</sup> The interaction of low-energy, high-repetition-rate pulsed lasers with photorefractive materials in the two-beam coupling configuration has been studied theoretically,<sup>6</sup> and the resulting coupled equations have been solved in terms of the coherence functions of the incident fields. This theory describes multiple-pulse effects and the cumulative buildup of the internal electric fields that are responsible for the spatial modulation of the refractive index. It predicts that photorefractive properties are independent of the pulse duration, as long as the pulse energy and bandwidth are not excessive.

In this Letter, we describe the nonlinear interaction of femtosecond pulses with barium titanate ( $\text{BaTiO}_3$ ) using a dispersion-compensated colliding-pulse mode-locked (CPM) laser. We demonstrate femtosecond temporal information storage and explore the factors that determine temporal resolution. Experiments using stimulated photon echoes<sup>7-9</sup> have demonstrated the possibility of storing temporal information in the frequency domain, with the use of inhomogeneously broadened atomic systems. The technique that we present here is more closely related to femtosecond holography.<sup>10</sup> In femtosecond holography, a spatial distribution of interference gratings results from the different intersection points of the temporal features of the writing and reference beams. This is the approach taken by Dominic *et al.*<sup>11</sup> to perform autocorrelation measurements of picosecond pulses using photorefractive materials. Conversely, it is also possible to use femtosecond holography to convert spatial features into temporal features.

We develop a simple geometrical model to describe our experimental results. The model involves parameters such as the beam waist at the crystal, the beam intersection angle, and the longitudinal length of the pulses (pulse duration  $t_p$  multiplied by the speed of light). Similar models have been used to explain the results of an experiment with photorefractive materials in which beams having partial spatial coherence were used<sup>12</sup> and can also be applied to describe temporal limitations of autocorrelation measurements of femtosecond pulses by noncollinear second-harmonic generation.

In order to explore the possibility of temporal information storage, we have used the experimental setup shown in Fig. 1. We use a reference beam and a signal beam. The CPM laser generates 50-fs pulses at a center wavelength of 625 nm and a pulse repetition rate of 100 MHz. A Michelson interferometer (M.I.) is used to generate a signal beam with pairs of copropagating pulses separated by a variable time delay  $T$ . The average powers used in our measurements were typically 1 mW in the reference beam and  $150(\times 2)$   $\mu\text{W}$  in the signal (double-pulse)

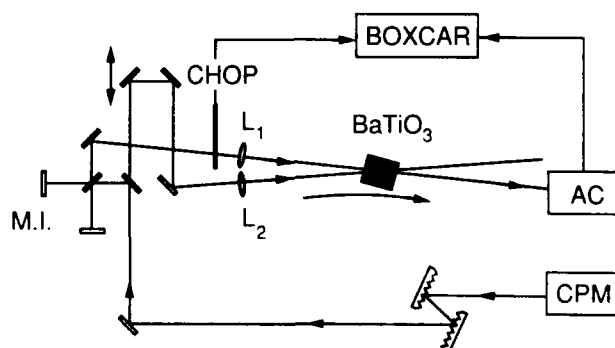


Fig. 1. Output of a CPM laser is prechirped by a grating pair and subsequently divided in two beams of variable relative delay. A boxcar averager, chopper, and autocorrelator (AC) are used to measure the duration of the pulses after the  $\text{BaTiO}_3$  crystal.

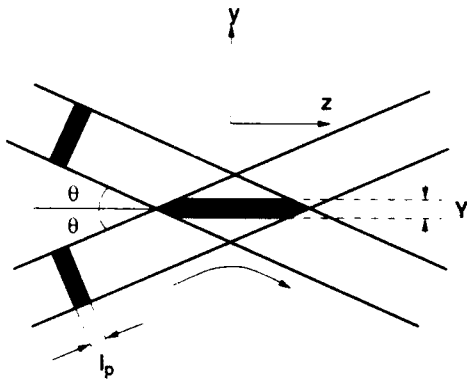


Fig. 2. Longitudinal length of the pulse  $l_p = ct_p$  determines the effective interaction region—defined by  $Y = l_p/\sin \theta$ —in the limit of large beam diameter ( $\omega_0/\cos \theta \gg Y$ ). In the small-beam-diameter limit ( $\omega_0/\cos \theta \ll Y$ ), the effective interaction region is determined by the intersection of the incident beams.

beam. The use of a grating pair is essential in order to precompensate for the material dispersion. Without dispersion compensation, the pulses broaden to approximately 200 fs in a single pass through the 5-mm BaTiO<sub>3</sub> crystal. The beam diameter could be varied by using lenses L1 and L2.

Temporal information reconstruction is investigated. A boxcar averager combined with a chopper allows the pulse, which is scattered off the volume grating, to be measured when the copropagating signal beam is blocked by taking advantage of the long decay time of the gratings. The relatively long dark period determined by the chopper ( $\sim 1$  ms) also ensures that free carrier gratings do not take part in the scattering process. It was noted that the buildup time and the coupling efficiency of the grating under femtosecond excitation is roughly the same as when a cw He-Ne laser with approximately the same average power is used.

To understand the role of the geometrical factors that influence temporal information encoding and reconstruction, let us consider the intersection region of two beams in the crystal as shown in Fig. 2. If we designate the wave vectors of the incident beams  $k_1$  and  $k_2$ , the Bragg condition is met by light scattered in directions  $k_2$  and  $k_1$ , respectively, as long as the spectral content of the incident pulses is small. The height  $Y$  of the effective interaction region in this large beam diameter case is determined by  $l_p/\sin \theta$ , where  $l_p = ct_p$  is the longitudinal pulse length. From Fig. 2 it is clear that if the pulse delay  $t$  is changed by a small amount, the volume grating will be formed at a slightly different  $y$  position. Conversely, if the beam diameter is small compared with the longitudinal length, the geometric overlap region of the beams is small and restricts the region in which the volume grating can form. These considerations define two limiting cases that we explore: large beam diameter ( $\omega_0/\cos \theta > l_p/\sin \theta$ ) and small beam diameter ( $\omega_0/\cos \theta < l_p/\sin \theta$ ).

In order to explore temporal broadening effects in the diffraction process, we first performed a single-pulse (one arm of the Michelson interferometer

blocked) experiment. The beam diameter at the crystal was set to  $\sim 2$  mm. For  $t_p = 50$  fs and  $\theta = 3$  deg,  $\omega_0/\cos \theta > l_p/\sin \theta$ , and the mixing is in the large-beam-diameter case where the effective interaction length is smaller than the region of the beam overlap. Figure 3(a) shows the autocorrelation of the input pulses (after they pass through the crystal), while the autocorrelation of the scattered reconstructed pulse is shown in Fig. 3(b). There is a small but noticeable broadening in this case. On the other hand, when the two lenses ( $f = 15$  cm) L1 and L2 are introduced, the beam waist is reduced to  $\omega_0 = 30$   $\mu$ m. Now  $\omega_0 \cos \theta < l_p/\sin \theta$ , and the mixing is in the small-beam-diameter case. In this case the autocorrelation of the scattered pulses shows almost no temporal broadening as seen in Fig. 3(c).

To demonstrate femtosecond temporal information storage, we use the double-pulse scheme de-

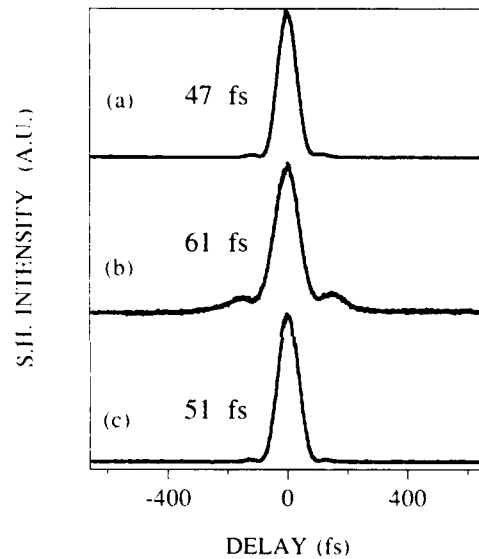


Fig. 3. (a) Autocorrelation trace of the prechirped pulses after a single pass through the crystal. The autocorrelation of the scattered pulses in the large- and small-beam-diameter limits is shown in (b) and (c), respectively. S.H., second harmonic.

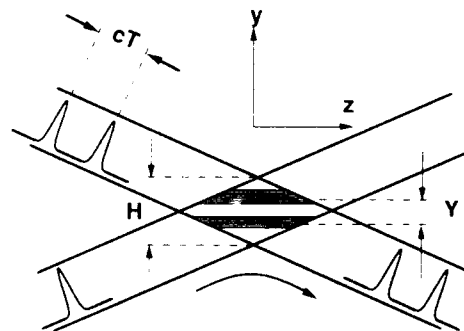


Fig. 4. Diagram showing that when the temporal separation  $T$  between the double pulses on one of the beams is sufficiently small relative to the beam intersection region, temporal information encoding is possible.

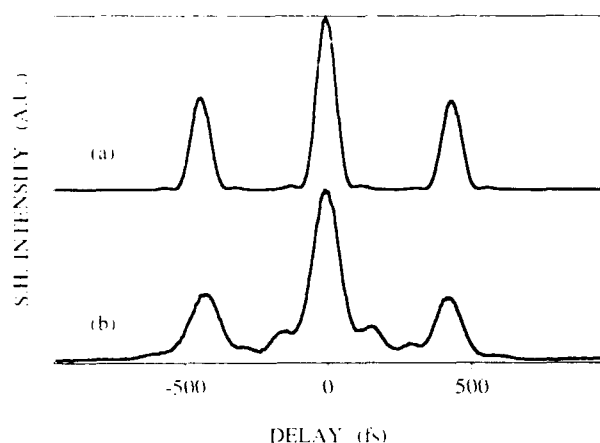


Fig. 5. (a) Autocorrelation of the prechirped double pulses after a single pass through the crystal. (b) The autocorrelation of the single pulse scattered from the double gratings.

scribed above. The situation that we consider is depicted in Fig. 4. When sufficiently large-beam diameters are used, more than one refractive index grating can be created in the photorefractive material. In order to encode information, the height  $Y$  of the effective interaction region must be much smaller than that of the beam-crossing region  $H$ , i.e.,  $\omega_0/\cos\theta > cT/\sin\theta \gg l_p/\sin\theta$ , and therefore the lenses L1 and L2 are not used. For the parameters of our experiment, the maximum pulse separation for which two independent volume gratings can be recorded in the crystal is of the order of  $T < \omega_0 \tan\theta/c \approx 1.0$  ps.

In Fig. 5(a) we show the autocorrelation of the incident double pulses for a temporal separation  $T$  of 450 fs. In Fig. 5(b) the autocorrelation trace of the reconstructed scattered pulses shows that the reproduction of the incoming pulses is reasonably good, although the wings of the input pulses are more evident in the scattered pulses and some broadening is observed. From the previous arguments, it can be predicted that if the lenses are used we would obtain only a single scattered pulse because the beam intersection region is now too small to support two distinct volume gratings as is in fact observed in our experiments.

An interesting aspect of this double-pulse experiment is that the near field of the scattered pulses (observed by blocking the double writing pulses) is a spatial replica of the volume gratings. The near field shows parallel bars produced by the scattering of the reference pulse from the stored gratings. The bars are perpendicular to the plane of the incident beams, and their separation changes in conjunction with the temporal pulse separation. These bars are observed because the intersection region of

the incoming beams is greater than the crystal length (along the propagation direction).

In summary, we have performed the first studies of femtosecond induced gratings in a photorefractive material. Temporal information encoding and reconstruction have been demonstrated. Pulse broadening and temporal information storage behavior are commensurate with a simple geometrical model that uses spatially distributed volume gratings.

This research was supported in part by U.S. Air Force Office of Scientific Research grant F43620-88C-0089, Joint Services Electronics Program contract DAAL03-89-C-0001, U.S. Office of Naval Research contract N00014-91-J-1956, National Science Foundation Presidential Young Investigator Program contracts 8552701-ECS and 8658025-ECS, and U.S. Army Research Office contract DAAL03-91-G-0243. L. H. Acioli acknowledges support from the Conselho Nacional de Pesquisas, Brazil.

M. Ulman is with the Department of Physics, Massachusetts Institute of Technology.

\*Permanent address, Departamento de Física, Universidade Federal de Pernambuco, Recife PE, Brazil.

## References

1. M. Cronin-Golomb, B. Fischer, J. O. White, and A. Yariv, *IEEE J. Quantum Electron.* **QE-20**, 12 (1984).
2. T. F. Boggess, J. O. White, and G. C. Valley, *J. Opt. Soc. Am. B* **7**, 2255 (1990).
3. G. Pauliat and G. Rosen, *J. Opt. Soc. Am. B* **7**, 2259 (1990).
4. A. M. Johnson, A. M. Glass, W. M. Simpson, R. B. Bylsma, and D. H. Olson, in *Digest of Optical Society of America Annual Meeting*, Vol. 11 of 1988 OSA Technical Digest Series (Optical Society of America, Washington, D.C., 1989), p. 128.
5. R. Trebino, C. C. Hayden, A. M. Johnson, W. M. Simpson, and A. M. Levine, *Opt. Lett.* **15**, 1079 (1990).
6. X. S. Yao, V. Dominic, and J. Feinberg, *J. Opt. Soc. Am. B* **7**, 2347 (1990).
7. T. Mossberg, *Opt. Lett.* **7**, 77 (1982).
8. S. Kroll, L. E. Jusinski, and R. Kachru, *Opt. Lett.* **16**, 517 (1991).
9. V. L. da Silva, Y. Silberberg, J. P. Heritage, E. W. Chase, M. A. Saifi, and M. J. Andrejco, in *Digest of Conference on Quantum Electronics and Laser Science* (Optical Society of America, Washington, D.C., 1991), paper QFD4.
10. J. A. Valdmanis, H. Chen, E. N. Leith, Y. Chen, and J. L. Lopez, in *Digest of Conference on Lasers and Electro-Optics* (Optical Society of America, Washington, D.C., 1990), paper CTUA1.
11. V. Dominic, X. S. Rao, and J. Feinberg, *Appl. Phys. Lett.* **56**, 521 (1990).
12. H. Kong, C. Wu, and M. Cronin-Golomb, *Opt. Lett.* **16**, 1183 (1991).

# Carrier diffusion effects in time-resolved photoluminescence

D. W. Bailey

Department of Electrical and Computer Engineering, University of South Carolina, Columbia, South Carolina 29208

C. J. Stanton

Department of Physics, University of Florida, Gainesville, Florida 32611

(Received 22 July 1991; accepted for publication 29 November 1991)

We model time-resolved photoluminescence in GaAs using an ensemble Monte Carlo method coupled with a  $k \cdot p$  calculation of the band structure. We show that on a picosecond scale, carrier diffusion perpendicular to the layer significantly reduces the density at the surface and consequently has a first-order effect on luminescence measurements. To illustrate this we compare the calculated luminescence, with and without diffusion, to experimental data.

Time-resolved photoluminescence, as recently demonstrated,<sup>1-5</sup> is an excellent method for measuring carrier relaxation in GaAs. By measuring the time and energy dependence of the luminescence with subpicosecond resolution, electron and hole distribution functions can be probed on the time scale during which thermalization occurs. By studying these systems, detailed information can be obtained about band structure, scattering rates, and nonequilibrium relaxation processes.

Quantitative analysis of time-resolved luminescence in GaAs is difficult, however, owing to many different scattering mechanisms and complex band structure. In this paper, we show that an additional effect, *carrier diffusion* perpendicular to the layer, must be included to accurately interpret the luminescence spectra on a picosecond scale. That is, the density of carriers at the surface decreases in time due to diffusion into the sample. This has a striking effect on the shape of time-resolved luminescence.

Our results show that by omitting diffusion in the analysis, the carrier density is likely to be overestimated in time-resolved luminescence experiments. This can be seen from the evolution of the carrier spatial profile, and from the calculated distribution functions with and without diffusion. We show that diffusion has a strong influence on the luminescence at different energies and show that it must be included to match the experimental data.

Our calculational approach uses an ensemble Monte Carlo method<sup>6,7</sup> to model photoexcited electron and hole dynamics. The hole band structure, optical matrix elements, density of states, region of photoexcitation, and Bloch overlap factors are determined from a 30-band  $k \cdot p$  calculation.<sup>8</sup> The initial photoexcited electron-hole pair states in the Monte Carlo simulation are determined according to the absorption of a monoenergetic pulse with a 0.5 ps full width at half maximum. The time-dependent distribution functions obtained from the Monte Carlo simulation are then used to calculate the time-dependent luminescence.

To include diffusion, the initial carrier spatial profile must be determined. The Monte Carlo method does not use a diffusion coefficient because the net redistribution of carriers depends directly on the transport parameters as given by the band structure and scattering rates. Thus, the

main ingredient for diffusion in our calculations is an initial concentration gradient.

In time-resolved luminescence, the photoexcitation pulse is incident on the surface of a semiconductor sample. Lateral diffusion is unimportant in picosecond measurements if the spot size is chosen large enough. The spatial distribution of carriers perpendicular to the layer is given by  $N_0 e^{-\alpha_0 x}$  for an instantaneous pulse, where  $N_0$  is the photoexcitation density, and where  $\alpha_0$ , the linear absorption coefficient, is  $4 \times 10^4 \text{ cm}^{-1}$  for 2.04 eV photoexcitation in GaAs.<sup>9</sup> That is, carriers are introduced into the Monte Carlo simulation according to the time dependence of the pulse at a  $k$  state and position determined by the absorption. For a pulse of finite duration, the carriers redistribute before the pulse is completed resulting in a more uniform profile.

The simulated spatial profile of photoexcited electrons is shown in Fig. 1 for a 0.5-ps pulse with  $N_0 = 3 \times 10^{18} \text{ cm}^{-3}$  in a 4600-Å layer of GaAs. Transparent confining layers are assumed. The 0-ps curve in Fig. 1 is lowest because at the center of the pulse only half of the total number of carriers are excited. After completion of the pulse, the total average density in the layer is  $N_0(1 - e^{-\alpha_0 L})/\alpha_0 L$ , where  $L$  is the thickness of the layer. The initial distribution is nearly exponential because carriers have little time to redistribute during a 0.5-ps pulse. Within several picoseconds, however, the carriers diffuse away from the surface and reduce the maximum density by half.

As shown in Fig. 1, the surface carrier density is changing during the rise time because of diffusion. It first quickly increases with the excitation pulse, and then decreases as carriers redistribute. The changing concentration complicates analysis of time-resolved luminescence measurements.

The expression for the luminescence is obtained by summing the number of photons over allowed optical transitions,

$$R(\omega, t) \propto \frac{1}{\omega} \int dt' W(t-t') \sum_{\mathbf{r}} \int d\mathbf{k} |H_{\mathbf{k}}|^2 \times \delta[E_c(\mathbf{k}) - E_v(\mathbf{k}) - \omega] f_c(\mathbf{k}, t') f_v(\mathbf{k}, t') \quad (1a)$$

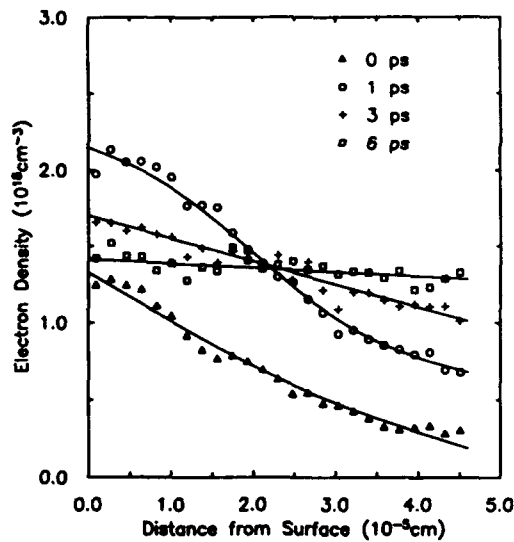


FIG. 1. Diffusion of electrons into a 4600-Å layer of GaAs photoexcited by a 0.5-ps pulse. Solid lines are drawn to guide the eye. Temporal center of the pulse is set at 0 ps. New carriers are initialized spatially according to  $3 \times 10^{18} e^{-\alpha_0 x} \text{ cm}^{-3}$ . Because the pulse is short, carriers do not redistribute much during the pulse and there is still a large gradient at 1 ps. Within several picoseconds, however, the electrons diffuse away from the surface and reduce the maximum density significantly.

$$\propto \frac{1}{\omega} \int dt' W(t-t') \sum_v |H_v(\omega)|^2 \times \rho_v(\omega) f_c(\omega, t') f_v(\omega, t'), \quad (1b)$$

where  $c$  and  $v$  denote conduction and valence bands,  $H(\omega)$  is the optical matrix element,  $\rho(\omega)$  is the joint density of states, and  $W(t)$  is a weighting factor that is determined by the time resolution of the experiment. That is, in the measurement the luminescence is sampled over a finite temporal window given by  $W(t)$ . A hyperbolic secant squared function with a full width half maximum of 0.5 ps is used in these simulations for  $W(t)$ . We assume collision broadening<sup>10</sup> and band-gap renormalization<sup>11</sup> are unimportant in picosecond measurements and neglect these effects in our model. We also assume that only carriers at the surface contribute to the luminescence, since photons emitted deep in the sample are reabsorbed before reaching the surface. If the sample thickness is much less than the absorption length, then all carriers can contribute to the luminescence and there are no diffusion effects. In these experiments, however, the sample is more than twice the absorption length of 0.2  $\mu\text{m}$ .<sup>12</sup>

The terms of most interest in Eq. 1(b) are  $f_c(\omega, t)$  and  $f_v(\omega, t)$ , the *isoenergy* distribution functions. These are the distribution functions averaged over the optically connected region.  $f(\omega, t)$  is a function of the luminescence energy, and is not the same as the *energy* distribution function,  $f(E, t)$ ; if conduction and valence bands are isotropic, then  $f(E, t)dE = f(\omega, t)d\omega$ . The heavy-hole band for GaAs, however, is highly anisotropic.<sup>13</sup> The *isoenergy* surface of  $\omega$  is determined by the sum of electron and hole energies for a given  $k$ . A measure of the time-resolved

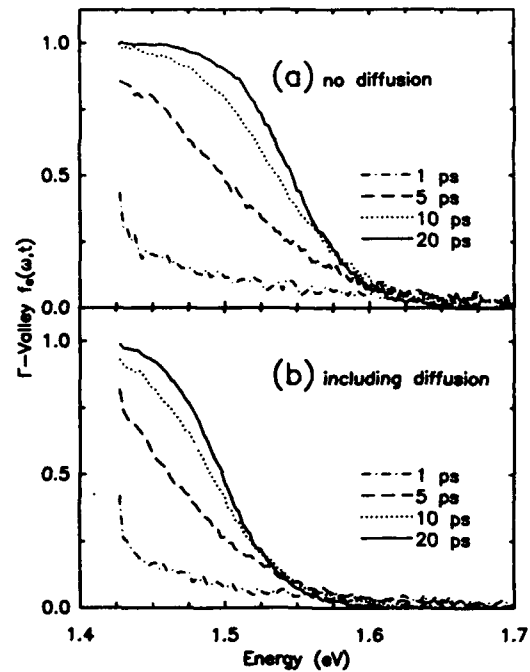


FIG. 2.  $\Gamma$ -valley electron isoenergy distributions as a function of luminescence energy photoexcited by a 0.5-ps, 2.04-eV pulse (a) omitting diffusion, and (b) including diffusion. Without diffusion the maximum carrier density is  $3 \times 10^{18} \text{ cm}^{-3}$ . Diffusion decreases  $f_c(\omega, t)$  significantly.

luminescence, then, is a measure of carrier dynamics, albeit in a nontrivial manner.

In Eq. (1), the recombination of electrons and heavy holes dominates the luminescence.<sup>5</sup> Heavy-, light-, and split-off hole dynamics are simulated, but the heavy holes control the luminescence because of their overwhelming number: at 1 ps after the center of the excitation pulse, the Monte Carlo simulation typically shows more than 95% of the hole population is in the heavy-hole band. Heavy holes have very high scattering rates,<sup>14</sup> so convergence of the distribution function occurs nearly by the end of the laser excitation pulse, especially at high density where hole-hole scattering is strong. Electrons provide virtually all of the structure on a picosecond scale, however, because they cool much slower than heavy holes. Electrons are excited at higher energy than the heavy holes, and inelastic scattering rates are much lower. Electron relaxation is also slower because intervalley scattering prevents a direct descent to the bottom of the  $\Gamma$  valley.<sup>6</sup>

Since electrons provide most of the structure of luminescence on a picosecond scale, in Fig. 2 we show  $f_c(\omega, t)$  at the surface in the  $\Gamma$  valley for two Monte Carlo simulations: (a) without diffusion, and (b) with diffusion. The area under  $f$  increases with time because the population in the  $\Gamma$  valley increases as carriers transfer from the satellite valleys. Comparing Fig. 2(a) with Fig. 2(b) shows that the occupation probability is less, and hence the surface density and the Fermi energy are less, when diffusion occurs. As Fig. 1 shows, the surface density is *decreasing* during the rise time of the luminescence. Diffusion thus has a significant influence on the distribution functions.

The importance of diffusion on the luminescence can

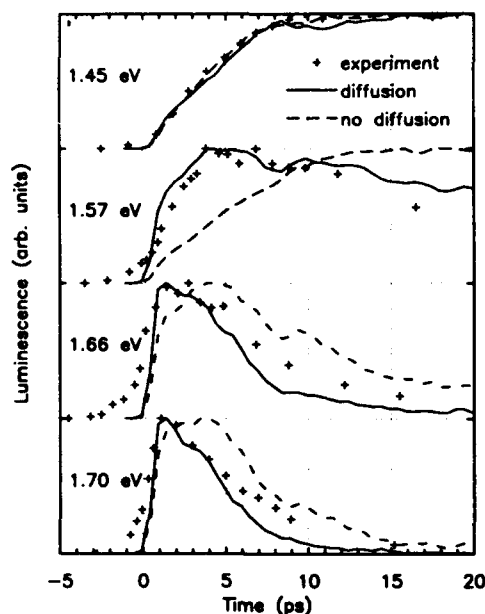


FIG. 3. Calculated luminescence in GaAs at 1.45, 1.57, 1.66, and 1.70 eV for the first 20 ps after  $3 \times 10^{18} \text{ cm}^{-3}$ , 0.5-ps, 2.04-eV photoexcitation compared with measurements by Block *et al.* (see Ref. 1). Experimental curves are time shifted, but the time scale is preserved. Characteristics of the experimental data are an increasing rise time for decreasing energy. The data follow this pattern strictly only when diffusion is included.

most easily be seen by comparisons at different energies. Figure 3 shows calculated luminescence for  $3 \times 10^{18} \text{ cm}^{-3}$  photoexcitation in GaAs at 1.45, 1.57, 1.66, and 1.70 eV with and without diffusion, along with time-resolved luminescence measurements digitized from Ref. 1. Generally, rise time and decay time of the luminescence decrease with energy. The calculations including diffusion agree better with the experiment than without diffusion. This is particularly evident at 1.57 eV, where without diffusion the luminescence does not decay.

Understanding Fig. 3 relies on an explanation of the decay of the initial transients. The luminescence does not appreciably deplete the carrier populations since for these experiments the recombination time is two to three orders of magnitude slower than the measurements. Any decay in the luminescence, therefore, is due to hot carriers relaxing to the band edge, that is, passing through the isoenergy surface.

With this in mind, Fig. 3 can be understood in terms of Figs. 1 and 2. Figure 1 shows diffusion decreases the surface density in the first 6 ps. At 1.70 and 1.66 eV in Fig. 3 this decreasing density accelerates the decay when diffu-

sion is included. At 1.57 eV without diffusion, Fig. 2 shows that  $f_c(\omega, t)$  is still increasing after 20 ps, thus causing the luminescence to steadily increase. With diffusion included, however, most of the states within a phonon energy below 1.57 eV are unoccupied, allowing electrons to continue relaxing and causing the luminescence to decay. At 1.45 eV there is no meaningful difference between luminescence rise times, because most states are occupied at low energy even with diffusion.

We have simulated time-resolved photoluminescence in GaAs by using a Monte Carlo method to model carrier transport and by calculating the recombination. Density of states, Bloch overlap factors, and optical matrix elements were determined by a  $\mathbf{k} \cdot \mathbf{p}$  method to realistically include hole band-structure effects. Our results show that including carrier diffusion in the analysis causes the surface concentration to change on a picosecond scale and be significantly lower than without diffusion. We compared our calculated luminescence with experimental data and showed that diffusion is a critical consideration.

We are grateful for useful discussions during the development of this work with K. Hess and B. Mason. M. Hohman provided technical assistance with several of the figures. This work was supported by the National Science Foundation through Grant No. DMR8957382 and by the U.S. Office of Naval Research through Grant No. N00091-J-1956. Supercomputing time has been provided by the National Center for Computational Electronics at the University of Illinois.

<sup>1</sup>D. Block, J. Shah, and A. C. Gossard, *Solid State Commun.* **59**, 527 (1986).

<sup>2</sup>J. Shah, B. Deveaud, T. C. Damen, W. T. Tsang, A. C. Gossard, and P. Lugli, *Phys. Rev. Lett.* **59**, 2222 (1987).

<sup>3</sup>J. Shah, *IEEE J. Quantum Electron.* **QE-24**, 276 (1988).

<sup>4</sup>W. W. Ruhle, K. Leo, and E. Bauser, *Phys. Rev. B* **40**, 1756 (1989).

<sup>5</sup>T. Elsaesser, J. Shah, L. Rota, and P. Lugli, *Phys. Rev. Lett.* **66**, 1757 (1991).

<sup>6</sup>D. W. Bailey, C. J. Stanton, and K. Hess, *Phys. Rev. B* **42**, 3423 (1990).

<sup>7</sup>C. J. Stanton, D. W. Bailey, and K. Hess, *Phys. Rev. Lett.* **65**, 231 (1990).

<sup>8</sup>F. H. Pollak, C. W. Higginbotham, and M. Cardona, *J. Phys. Soc. Jpn. Suppl.* **21**, 20 (1966).

<sup>9</sup>M. D. Sturge, *Phys. Rev.* **127**, 768 (1962).

<sup>10</sup>P. T. Landsberg, *Phys. Status Solidi* **15**, 623 (1966).

<sup>11</sup>W. F. Brinkman and T. M. Rice, *Phys. Rev. B* **7**, 1508 (1973).

<sup>12</sup>J. S. Blakemore, *J. Appl. Phys.* **53**, R123 (1982).

<sup>13</sup>J. D. Wiley, in *Semiconductors and Semimetals*, edited by R. K. Willardson and A. C. Beer (Academic, New York, 1971), Vol. 6, pp. 91-174.

<sup>14</sup>T. Brudevoll, T. A. Fjeldly, J. Baek, and M. S. Shur, *J. Appl. Phys.* **67**, 7373 (1990).



## Rate equations for the study of femtosecond intervalley scattering in compound semiconductors

C. J. Stanton

*Department of Physics, University of Florida, Gainesville, Florida 32611*

D. W. Bailey

*Department of Electrical and Computer Engineering, University of South Carolina, Columbia, South Carolina 29208*

(Received 30 September 1991; revised manuscript received 9 December 1991)

We present solutions to a set of rate equations for the electron dynamics after photoexcitation by a 2.0-eV laser in GaAs and InP. Results obtained, although simpler than full Monte Carlo solutions, closely follow the experimental data and provide insight into intervalley scattering. Calculations show that the net return time of electrons from the satellite  $L$  valleys into the  $\Gamma$  valley is not limited by the intervalley scattering rate, but is instead limited by the polar-optic-phonon scattering rate within the  $\Gamma$  valley. This shows that the time-dependent mobility and luminescence experiments depend on the  $L$ -valley depopulation rate, which differs from the  $L \rightarrow \Gamma$  intervalley scattering rate. Results further suggest that the  $\Gamma \rightarrow L$  scattering rate is faster than the polar-optic-phonon scattering rate.

## INTRODUCTION

Intervalley scattering in compound semiconductors is responsible for the transferred electron effect<sup>1</sup> and is thus important in the operation of Gunn oscillators and microwave devices. As a result, there is interest in accurately measuring the intervalley scattering rates. With the development of ultrafast lasers, experiments with a time resolution comparable to the intervalley scattering times have become possible. These experiments include the rise time of band-edge photoluminescence,<sup>2,3</sup> pump-infrared-probe absorption,<sup>4</sup> femtosecond reflectivity,<sup>5</sup> equal pulse correlation,<sup>6,7</sup> pump-continuum-probe absorption,<sup>8</sup> transient nonlinear absorption,<sup>9,10</sup> and cw acceptor luminescence.<sup>11-13</sup>

Several of these experiments claim to measure the deformation potential phonon scattering rate in GaAs for the scattering of carriers from the satellite  $L$  valleys back into the central  $\Gamma$  valley. The values reported for the deformation potential constant  $D_{\Gamma L}$ , however, have a large variance.<sup>13</sup> In this paper, we show, through a series of rate-equation models, that the time measured in some of these experiments is *not* the  $L \rightarrow \Gamma$  scattering rate, but the  $L$ -valley depopulation rate. This suggests that the apparent controversy is due in part to a misinterpretation of some of the experiments.

Comparison of our calculations to luminescence and mobility experiments shows that in GaAs, the  $L$ -valley depopulation rate is most strongly influenced by the rate of inelastic scattering, chiefly the polar-optic-phonon (POP) emission rate, *within* the  $\Gamma$  valley. If the inelastic scattering rate in the  $\Gamma$  valley is small compared to the  $\Gamma \rightarrow L$  scattering rate, then to lowest order, the  $L$ -valley depopulation rate *does not depend* on the  $L \rightarrow \Gamma$  rate. For this case, the bottleneck for the return of electrons from the satellite  $L$  valleys to the central  $\Gamma$  valley is the cooling of the electrons in the  $\Gamma$  valley. The cooling of electrons allows a net flow of electrons from the  $L$  valley

into the  $\Gamma$  valley. In addition, our studies show that the  $\Gamma \rightarrow L$  scattering rate is larger than the POP scattering rate.

This paper is organized as follows. We start with a two-state rate-equation model. While this model is too simple to describe optical experiments in GaAs, it illustrates an important point, namely that the two intervalley scattering rates  $\Gamma \rightarrow L$  and  $L \rightarrow \Gamma$  are *not independent* but are related through the density of states in each valley. We then extend our method to a three-state model. This allows us to describe actual experiments in GaAs provided that the measured quantities depend only on the valley the electrons occupy and not on the details of the electron states within each valley. (An example of such an experiment is the femtosecond mobility experiments of Nuss, Auston, and Capasso.<sup>5</sup>) Finally, we extend the three-state model to a four-state model. With four states, we can account for experiments that are sensitive not only to which valley the electrons occupy, but also are sensitive to which state within the valley the electron occupies. For example, in the time-resolved luminescence experiments of Shah *et al.*,<sup>2</sup> only electrons at the bottom of the conduction band contribute to the luminescence signal.

## TWO-STATE MODEL

We start with a two-state model shown in Fig. 1. It is the simplest possible model, but illustrates several key points about electron relaxation in compound semiconductors. One state represents all electrons in the  $\Gamma$  valley and the other represents all electrons that are in the  $L$  valleys.  $\gamma_{\Gamma L}$  is the  $\Gamma \rightarrow L$  scattering rate, and  $\gamma_{L\Gamma}$  is the  $L \rightarrow \Gamma$  scattering rate.

This is not a realistic model for carrier dynamics in compound semiconductors because it does not allow for states in the  $\Gamma$  valley that are not energetically able to scatter into the  $L$  valley. That is, relaxation of electrons

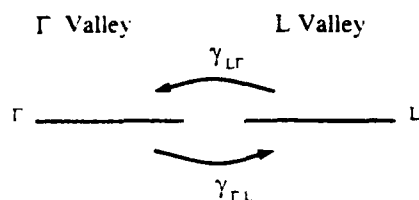


FIG. 1. The two-state model for intervalley scattering in compound semiconductors. The state  $\Gamma$  represents all electrons in the central  $\Gamma$  valley, while the state  $L$  represents all electrons in the  $L$  valleys. No distinction is made between electrons within a given valley.  $\gamma_{\Gamma L}$  is the  $\Gamma$  to  $L$  scattering rate and  $\gamma_{L\Gamma}$  is the  $L$  to  $\Gamma$  scattering rate.

in the  $\Gamma$  valley is ignored. Nonetheless, this model is instructive for the analysis of more complex systems and has features applicable to real systems.

The rate equations in this model are given in matrix form by

$$\frac{d}{dt} \begin{pmatrix} n_{\Gamma} \\ n_L \end{pmatrix} = \begin{pmatrix} -\gamma_{\Gamma L} & \gamma_{L\Gamma} \\ \gamma_{\Gamma L} & -\gamma_{L\Gamma} \end{pmatrix} \begin{pmatrix} n_{\Gamma} \\ n_L \end{pmatrix}. \quad (1)$$

Here  $n_{\Gamma}$  and  $n_L$  are the densities of electrons in the  $\Gamma$  and  $L$  valleys, respectively. A straightforward calculation shows that the eigenvalues and (unnormalized) eigenvectors are given by

$$\lambda_1 = 0, \quad \lambda_2 = -(\gamma_{\Gamma L} + \gamma_{L\Gamma}), \quad (2)$$

$$\mathbf{V}_1 = \begin{pmatrix} \gamma_{L\Gamma} \\ \gamma_{\Gamma L} \end{pmatrix}, \quad \mathbf{V}_2 = \begin{pmatrix} 1 \\ -1 \end{pmatrix}.$$

The zero eigenvalue results from the total density  $n_{\Gamma} + n_L$  being constant. The general solution to the two-state model is obtained by taking a superposition of the two eigensolutions:

$$\begin{pmatrix} n_{\Gamma}(t) \\ n_L(t) \end{pmatrix} = A \begin{pmatrix} \gamma_{\Gamma L} \\ \gamma_{L\Gamma} \end{pmatrix} + B \begin{pmatrix} 1 \\ -1 \end{pmatrix} e^{-(\gamma_{\Gamma L} + \gamma_{L\Gamma})t}. \quad (3)$$

The constants  $A$  and  $B$  are determined by the initial conditions:

$$\begin{pmatrix} \gamma_{L\Gamma} & 1 \\ \gamma_{\Gamma L} & -1 \end{pmatrix} \begin{pmatrix} A \\ B \end{pmatrix} = \begin{pmatrix} n_{\Gamma}^0 \\ n_L^0 \end{pmatrix}. \quad (4)$$

Here  $n_{\Gamma}^0$  and  $n_L^0$  are the initial populations of carriers in the two valleys. Solving Eq. (4) for  $A$  and  $B$ , we obtain the solution

$$n_{\Gamma}(t) = \frac{n_{\Gamma}^0 \gamma_{\Gamma L} - n_L^0 \gamma_{L\Gamma}}{\gamma_{\Gamma L} + \gamma_{L\Gamma}} + \left[ \frac{n_L^0 \gamma_{\Gamma L} - n_{\Gamma}^0 \gamma_{L\Gamma}}{\gamma_{\Gamma L} + \gamma_{L\Gamma}} \right] e^{-(\gamma_{\Gamma L} + \gamma_{L\Gamma})t}, \quad (5)$$

$$n_L(t) = \frac{n_L^0 \gamma_{\Gamma L} - n_{\Gamma}^0 \gamma_{L\Gamma}}{\gamma_{\Gamma L} + \gamma_{L\Gamma}} - \left[ \frac{n_L^0 \gamma_{\Gamma L} - n_{\Gamma}^0 \gamma_{L\Gamma}}{\gamma_{\Gamma L} + \gamma_{L\Gamma}} \right] e^{-(\gamma_{\Gamma L} + \gamma_{L\Gamma})t}.$$

The total number of carriers  $n = n_{\Gamma}(t) + n_L(t) = n_{\Gamma}^0 + n_L^0$  is independent of time.

In equilibrium ( $t \rightarrow \infty$ ) the number of carriers in each

valley is found to be

$$n_{\Gamma}^{\text{eq}} = n_{\Gamma}(t \rightarrow \infty) = \frac{n \gamma_{L\Gamma}}{\gamma_{\Gamma L} + \gamma_{L\Gamma}}, \quad (6)$$

$$n_L^{\text{eq}} = n_L(t \rightarrow \infty) = \frac{n \gamma_{\Gamma L}}{\gamma_{\Gamma L} + \gamma_{L\Gamma}}.$$

From this, one obtains a "detailed balance" relation

$$\frac{\gamma_{L\Gamma}}{\gamma_{\Gamma L}} = \frac{n_{\Gamma}^{\text{eq}}}{n_L^{\text{eq}}} \equiv R. \quad (7)$$

$R$  is defined to be the equilibrium ratio of the populations in the two valleys. If a more detailed model based on a complete description of all states were considered, then intervalley scattering events would obey a detailed balance relation given by

$$W_{\Gamma \rightarrow L}^{k, k'} f_{\Gamma}^{\text{eq}}(\mathbf{k}) = W_{L \rightarrow \Gamma}^{k', k} f_L^{\text{eq}}(\mathbf{k}'), \quad (8)$$

with  $W_{\Gamma \rightarrow L}^{k, k'}$  the transition probability per unit time from state  $\mathbf{k}$  in the  $\Gamma$  valley to state  $\mathbf{k}'$  in the  $L$  valley.<sup>14</sup> This means that the  $\Gamma \rightarrow L$  and  $L \rightarrow \Gamma$  rates are dependent. Knowledge of one implies knowledge of the other.

Another point to note is that deviations from the equilibrium populations relax with a rate given by the sum of the two scattering rates  $\gamma_{\Gamma L} + \gamma_{L\Gamma}$ . That is, if  $\delta n_{\Gamma}(t) \equiv n_{\Gamma}(t) - n_{\Gamma}^{\text{eq}}$ , then

$$\delta n_{\Gamma}(t) = \left[ \frac{n_{\Gamma}^0 \gamma_{\Gamma L} - n_L^0 \gamma_{L\Gamma}}{\gamma_{\Gamma L} + \gamma_{L\Gamma}} \right] e^{-(\gamma_{\Gamma L} + \gamma_{L\Gamma})t}, \quad (9)$$

$$\delta n_L(t) = -\delta n_{\Gamma}(t) = \left[ \frac{n_L^0 \gamma_{\Gamma L} - n_{\Gamma}^0 \gamma_{L\Gamma}}{\gamma_{\Gamma L} + \gamma_{L\Gamma}} \right] e^{-(\gamma_{\Gamma L} + \gamma_{L\Gamma})t}.$$

This counters the naive assumption that a deviation from the equilibrium population in the  $\Gamma$  valley relaxes with  $\gamma_{\Gamma L}$  and a deviation in the  $L$  valley relaxes with  $\gamma_{L\Gamma}$ . Any deviation from the equilibrium ratio of carriers will relax with the combined rate  $\gamma_{\Gamma L} + \gamma_{L\Gamma}$ . While this seems strange for electrons in the  $L$  valley where the  $L \rightarrow \Gamma$  scattering rate is slower than the  $\Gamma \rightarrow L$  rate, it is important to remember that fewer electrons have to transfer from the  $L$  valley to restore the equilibrium ratio. Equation (9) means that the carrier densities in the two valleys equilibrate on a time scale comparable to the fastest of the two scattering times.

### THREE-STATE MODEL

The two-state model is simplistic since it does not consider that the  $\Gamma$  valley is made up of several states. In particular, there is an energy threshold within the  $\Gamma$  valley below which electrons can no longer scatter into the satellite  $L$  valleys. A more realistic model for intervalley transfer must allow for this. Such a model is given by the three-state model shown in Fig. 2. In the three-state model, states in the  $\Gamma$  valley are separated above and below  $\Delta$ , the energy threshold for transfer into the  $L$  valley. All  $\Gamma$  valley electrons with enough energy to transfer into the  $L$  valleys are in the  $\Gamma^>$  state; all  $\Gamma$  valley electrons with energy less than  $\Delta$  are in the  $\Gamma^<$  state; and

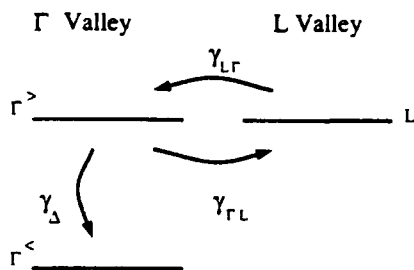


FIG. 2. The three-state model for intervalley scattering.  $\Gamma^+$  is the state that represents all electrons in the  $\Gamma$  valley which are energetically able to transfer into the  $L$  valley state. The  $\Gamma^-$  state represents all electrons in the  $\Gamma$  valley that do not have enough energy to transfer to the  $L$  valley state. Scattering from the  $\Gamma^+$  state to the  $\Gamma^-$  state occurs via inelastic scattering within the  $\Gamma$  valley with a rate  $\gamma_\Delta$ . This occurs mostly by POP emission.

electrons in the  $L$  valley are in the third state. Only electrons in state  $\Gamma^+$  can scatter into the  $L$ -valley state and electrons in the  $L$ -valley state can only scatter into the  $\Gamma^+$  state. Scattering from the  $\Gamma^+$  state into the  $\Gamma^-$  state is given by the scattering rate  $\gamma_\Delta$  and occurs through inelastic scattering within the  $\Gamma$  valley. This is chiefly through POP emission.<sup>15</sup> While POP absorption makes scattering from below  $\Delta$  to above  $\Delta$  possible, for simplicity it is ignored in this model because POP emission occurs more frequently.

Note that for simplicity we have not included scattering into the satellite  $X$  valleys. For 2.0-eV photoexcitation experiments, only a small fraction of the photoexcited electrons are energetically able to scatter into the  $X$  valleys so that this is a minor correction. For higher energies, the  $X$  valleys must be included, or the satellite valley state (and hence the appropriate scattering rates) modified to include both  $L$  and  $X$  valleys. Inclusion of an  $X$  valley should be straightforward.

The equations for the three-state model are given by

$$\frac{d}{dt} \begin{bmatrix} n_{\Gamma^+}(t) \\ n_L(t) \\ n_{\Gamma^-}(t) \end{bmatrix} = \begin{bmatrix} -(\gamma_{\Gamma L} + \gamma_\Delta) & \gamma_{L\Gamma} & 0 \\ \gamma_{\Gamma L} & -\gamma_{L\Gamma} & 0 \\ \gamma_\Delta & 0 & 0 \end{bmatrix} \begin{bmatrix} n_{\Gamma^+}(t) \\ n_L(t) \\ n_{\Gamma^-}(t) \end{bmatrix} \quad (10)$$

The eigenvalues are

$$\begin{aligned} \lambda_0 &= 0, \\ \lambda_{\pm} &= -\frac{1}{2} \left[ (\gamma_{\Gamma L} + \gamma_{L\Gamma} + \gamma_\Delta) \right. \\ &\quad \left. \pm \sqrt{(\gamma_{\Gamma L} + \gamma_{L\Gamma} + \gamma_\Delta)^2 - 4\gamma_{L\Gamma}\gamma_\Delta} \right]. \end{aligned} \quad (11)$$

The unnormalized eigenvectors for the matrix in the three state model are given by

$$\begin{aligned} \mathbf{V}_0 &= \begin{bmatrix} 0 \\ 0 \\ \gamma_\Delta \end{bmatrix}, \\ \mathbf{V}_+ &= \begin{bmatrix} \lambda_+ \\ \frac{\gamma_{\Gamma L}\lambda_+}{\gamma_{L\Gamma} + \lambda_+} \\ \gamma_\Delta \end{bmatrix}, \\ \mathbf{V}_- &= \begin{bmatrix} \lambda_- \\ \frac{\gamma_{\Gamma L}\lambda_-}{\gamma_{L\Gamma} + \lambda_-} \\ \gamma_\Delta \end{bmatrix}. \end{aligned} \quad (12)$$

The general solution is

$$\begin{bmatrix} n_{\Gamma^+}(t) \\ n_L(t) \\ n_{\Gamma^-}(t) \end{bmatrix} = A\mathbf{V}_0 + B\mathbf{V}_+e^{\lambda_+t} + C\mathbf{V}_-e^{\lambda_-t}, \quad (13)$$

with  $A$ ,  $B$ , and  $C$  determined by the initial conditions

$$\begin{bmatrix} 0 & \lambda_+ & \lambda_- \\ 0 & \frac{\gamma_{\Gamma L}\lambda_+}{\gamma_{L\Gamma} + \lambda_+} & \frac{\gamma_{\Gamma L}\lambda_-}{\gamma_{L\Gamma} + \lambda_-} \\ \gamma_\Delta & \gamma_\Delta & \gamma_\Delta \end{bmatrix} \begin{bmatrix} A \\ B \\ C \end{bmatrix} = \begin{bmatrix} n_{\Gamma^+}^0 \\ n_L^0 \\ n_{\Gamma^-}^0 \end{bmatrix}. \quad (14)$$

Solving for  $A$ ,  $B$ , and  $C$  and using the relations

$$\begin{aligned} \lambda_+ \lambda_- &= \gamma_{L\Gamma} \gamma_\Delta, \\ (\gamma_{L\Gamma} + \lambda_+)(\gamma_{L\Gamma} + \lambda_-) &= -\gamma_{\Gamma L} \gamma_{L\Gamma}, \end{aligned} \quad (15)$$

we can find the final solution for the populations of the three states. For the experiments we are considering,<sup>2,5</sup> electrons are initially excited only into the  $\Gamma^+$  state, i.e.,  $n_{\Gamma^+}^0 \neq 0$ ,  $n_L^0 = 0$ ,  $n_{\Gamma^-}^0 = 0$ ; then

$$\begin{aligned} n_{\Gamma^+}(t) &= n_{\Gamma^+}^0 \left[ \left( \frac{\gamma_{L\Gamma} + \lambda_+}{\lambda_+ - \lambda_-} \right) e^{\lambda_+t} - \left( \frac{\gamma_{L\Gamma} + \lambda_-}{\lambda_- - \lambda_+} \right) e^{\lambda_-t} \right], \\ n_L(t) &= n_{\Gamma^+}^0 \left[ \left( \frac{\gamma_{\Gamma L}}{\lambda_+ - \lambda_-} \right) (e^{\lambda_+t} - e^{\lambda_-t}) \right], \\ n_{\Gamma^-}(t) &= \frac{n_{\Gamma^+}^0 \gamma_\Delta}{\lambda_+ - \lambda_-} \left[ \left( \frac{\gamma_{L\Gamma} + \lambda_-}{\lambda_+} \right) (e^{\lambda_+t} - 1) \right. \\ &\quad \left. - \left( \frac{\gamma_{L\Gamma} + \lambda_-}{\lambda_-} \right) (e^{\lambda_-t} - 1) \right]. \end{aligned} \quad (16)$$

Some insight into the intervalley problem is obtained by looking at the limiting form for the eigenvalues in Eq. (11). As mentioned earlier, the detailed balance relation requires that  $\gamma_{\Gamma L}$  and  $\gamma_{L\Gamma}$  be in the ratio of the equilibrium populations  $R$ . Taking into account nonparabolicity of the  $\Gamma$  valley and the fourfold degeneracy of the  $L$  valleys,<sup>16</sup> for 2-eV photoexcitation in GaAs, electrons are photoexcited 0.5 eV above the bottom of the conduction band<sup>17,18</sup> and

$$R \equiv \frac{\gamma_{L\Gamma}}{\gamma_{\Gamma L}} = \frac{n_{\Gamma}^{\text{eq}}}{n_{L}^{\text{eq}}} \approx 0.1. \quad (17)$$

This ratio is large because the effective mass in the  $L$  valley is substantially greater than the effective mass in the  $\Gamma$  valley.<sup>19</sup> We also note that *nonparabolicity* is an important consideration in determining this ratio since at 0.5 eV nonparabolicity increases the density of states by 60% in the  $\Gamma$  valley.<sup>20</sup>

Because of the large value of  $R$ , it follows that  $\gamma_{L\Gamma} \ll \gamma_{\Gamma L}$  and the square root in Eq. (11) can be expanded to yield

$$\lambda_{+} \approx -(\gamma_{\Gamma L} - \gamma_{\Delta}), \quad \lambda_{-} \approx \frac{-\gamma_{L\Gamma}\gamma_{\Delta}}{\gamma_{\Gamma L} + \gamma_{\Delta}}. \quad (18)$$

Note that for nonzero rates  $|\lambda_{+}| \gg |\lambda_{-}|$ .

There are two interesting cases depending on how the  $\Gamma \rightarrow L$  intervalley scattering rate compares with the inelastic scattering rate in the  $\Gamma$  valley. In the limit that  $\gamma_{\Delta} \ll \gamma_{\Gamma L}$ , i.e.,  $\Gamma \rightarrow L$  intervalley scattering is faster than POP scattering within the  $\Gamma$  valley, then

$$\lambda_{-} \approx -\frac{\gamma_{L\Gamma}}{\gamma_{\Gamma L}} \gamma_{\Delta} = -\frac{n_{\Gamma}^{\text{eq}}}{n_{L}^{\text{eq}}} \gamma_{\Delta} = -R \gamma_{\Delta}. \quad (19)$$

In this case,  $\lambda_{-}$  does not measure the  $L \rightarrow \Gamma$  scattering rate, but instead measures the product of the inelastic-scattering rate and the ratio of the equilibrium populations  $R$ . Even though  $\gamma_{\Delta}$  might be greater than  $\gamma_{L\Gamma}$ , the net return of electrons from the  $L$  valleys is determined by how fast electrons relax to lower-energy levels within the  $\Gamma$  valley, not on how fast they scatter from the  $L$  valley to  $\Gamma$  valley.

For  $\gamma_{\Delta} \gg \gamma_{\Gamma L}$ , i.e., POP scattering is faster than the  $\Gamma \rightarrow L$  rate, we obtain

$$\lambda_{-} \approx -\gamma_{L\Gamma}. \quad (20)$$

This is, if electrons in the  $\Gamma$  valley are rapidly scattered to low-energy states, then the return time of the  $L$ -valley electrons is limited by the  $L \rightarrow \Gamma$  scattering rate. Only in this limit does the  $L$ -valley depopulation rate measure the  $L \rightarrow \Gamma$  scattering rate.

It is interesting to note that, although the scattering rates given by the  $\gamma$ 's in this model are constants, the densities given in Eq. (16) are not characterized by a single exponential decay. Therefore the depopulation rate of a given state [given by  $-d \ln(n)/dt$ ] is time dependent in spite of the fact that the scattering rates are constant. Furthermore, depending on the values for the scattering rates, the two eigenvalues  $\lambda_{+}$  and  $\lambda_{-}$  can differ by more than an order of magnitude, which leads to depopulation rates that can change rapidly on a short time scale. Thus the total number of scattering events from the  $\Gamma$  to  $L$  valley, which is proportional to  $n_{\Gamma}(t)\gamma_{\Gamma L}$ , changes rapidly with time after the initial photoexcitation in agreement with earlier Monte Carlo calculations.<sup>21,22</sup> This change, however, reflects the time dependence of  $n_{\Gamma}(t)$  and not the scattering rate  $\gamma_{\Gamma L}$ .

The three-state model can be applied to a large number of experiments that are sensitive primarily to which valley the electron populates. An example of such an experiment is that of Nuss, Auston, and Capasso (NAC).<sup>5</sup> In the NAC experiment,<sup>5</sup> the time-dependent reflectivity was measured on a femtosecond scale to infer the electron mobility as a function of time. Since the mobility of electrons in the  $\Gamma$  valley is nearly independent of energy, and the mobility of electrons in the  $L$  valleys is negligible by comparison,<sup>19</sup> a measure of the mobility as a function of time is a measure of the density of electrons in the  $\Gamma$  valley (without regard to which state within the  $\Gamma$  valley the electrons occupy). In the three-state model, the mobility is therefore proportional to

$$\frac{\mu(t)}{\mu(t \rightarrow \infty)} = \frac{n_{\Gamma}(t) + n_{\Gamma'}(t)}{n_{\Gamma}^0}. \quad (21)$$

To compare our calculations to the experiment, we must estimate the scattering rates. Based on the scattering rates of Schichijo and co-workers,<sup>23,24</sup> we estimate the rates to be given by

$$\begin{aligned} \gamma_{\Gamma L} &= 2 \times 10^{13} \text{ s}^{-1}, \\ R &\equiv \frac{\gamma_{L\Gamma}}{\gamma_{\Gamma L}} = 0.1, \\ \gamma_{\Delta} &= 5 \times 10^{12} \text{ s}^{-1}. \end{aligned} \quad (22)$$

In a later section, we show the sensitivity of the results to these values. The results of the three-state calculation are plotted in Figs. 3–6.

In Fig. 3, the experimental mobility from the NAC experiment<sup>5</sup> is shown as the solid line. The calculated

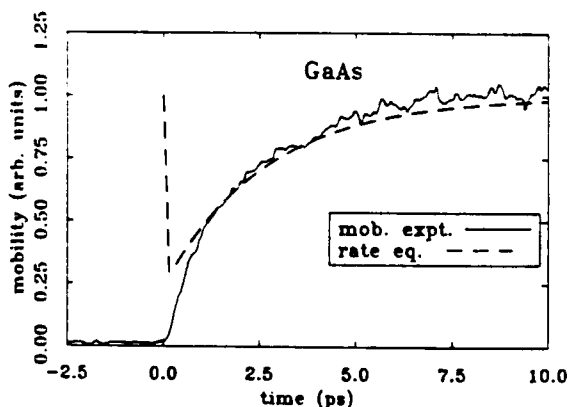


FIG. 3. The mobility vs time for GaAs as calculated from the three-state model. The solid line is the experimental work of Nuss, Auston, and Capasso (Ref. 5), the dashed line is the result from the three-state model. It is assumed that the mobility of electrons in the  $L$  valleys is close to zero while the mobility of the electrons in the  $\Gamma$  valley is independent of energy. The mobility is therefore proportional to the number of electrons in the  $\Gamma$  valley  $[n_{\Gamma}(t) + n_{\Gamma'}(t)]$ . The initial peak in the rate equation solution near  $t=0$  results from electrons initially photoexcited in the  $\Gamma$  valley that rapidly transfer into the  $L$  valley. This occurs on an extremely fast time scale and is not resolvable in the experimental data.

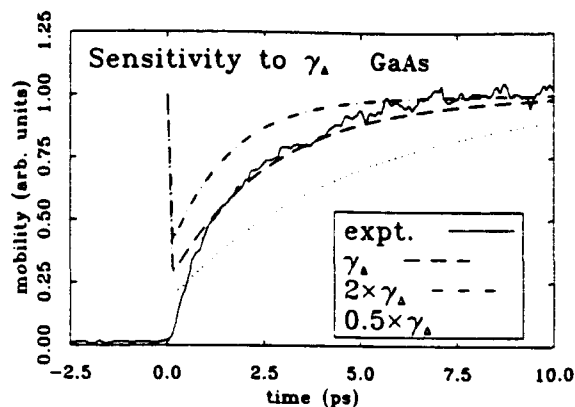


FIG. 4. Sensitivity of the rise time of the mobility to the inelastic (POP) scattering rate  $\gamma_{\Delta}$ . The solid line is the experimental data (Ref. 5), the dashed line the results of the three-state rate-equation model. For the dash-dotted line, the rate is doubled, whereas for the dotted line, the rate is cut in half. As can be seen, the rise time of the mobility is very sensitive to this quantity.

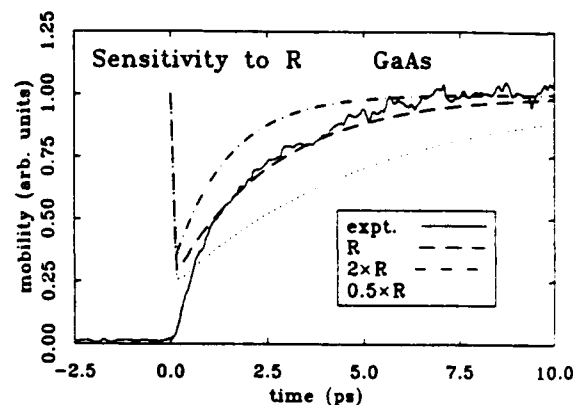


FIG. 6. Sensitivity of the rise time of the mobility to the equilibrium population ratio  $R$ . For the dash-dotted line, the  $L$  to  $\Gamma$  rate  $\gamma_{L\Gamma}$  is doubled keeping  $\gamma_{\Gamma L}$  constant and thus doubling the equilibrium population ratio  $R$ . For the dotted line, the ratio  $R$  is halved. As can be seen, the rise time of the mobility is very sensitive to this ratio.

curve from the three-state model, Eq. (21), is shown as the dotted line. The two are in close agreement a short time after  $t=0$ . The peak in the rate equation model near  $t=0$  is caused by electrons initially excited in the  $\Gamma$  valley that quickly scatter to the  $L$  valleys. This fast initial transient is not resolvable in the experimental data and indicates that the initial  $\Gamma \rightarrow L$  transfer is rapid.

To test the sensitivity of the rate equation model, we vary the parameters. In Fig. 4, we show the sensitivity of the rise time of the mobility to the POP scattering rate  $\gamma_{\Delta}$ . The solid line corresponds to the experimental data

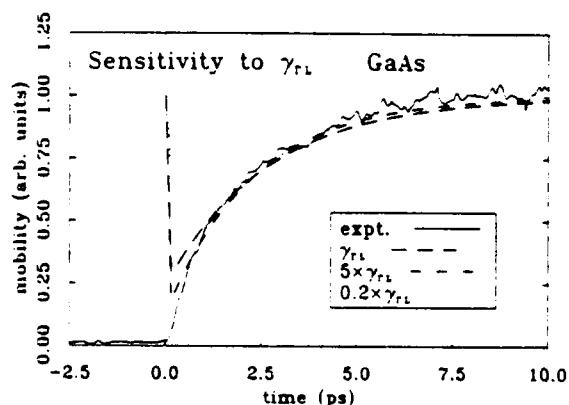


FIG. 5. Sensitivity of the rise time of the mobility to the intervalley scattering time  $\gamma_{\Gamma L}$ . The solid line is the experimental data (Ref. 5) and the dashed line the calculation. For the dash-dotted line, the intervalley rate  $\gamma_{\Gamma L}$  is increased by a factor of 5 as well as the  $L$  to  $\Gamma$  rate  $\gamma_{L\Gamma}$ , thus keeping the ratio  $R$  constant. As can be seen a fivefold increase does not significantly influence the results indicating the general insensitivity of the rise time to the intervalley scattering. When the rates are divided by a factor of 5, the dotted line results. When divided by a factor of 5, the intervalley scattering rate is slower than the POP rate and thus shows some discrepancy with the experiment at short times.

of NAC, and the dashed line to the previous fit based on the rate-equation model (cf. Fig. 3). For the dash-dotted line, the POP rate is doubled, whereas for the dotted line, the POP rate is cut in half. As can be seen, the mobility and hence the number of electrons in the  $\Gamma$  valley depends strongly on the POP scattering rate. If the POP scattering rate is low,  $\gamma_{\Delta} \ll \gamma_{\Gamma L}$ , then according to Eq. (19), it takes longer to get a net transfer of electrons back into the (high mobility)  $\Gamma$  valley.

In Fig. 5, we show the sensitivity of the rise time of the mobility to the intervalley scattering rates. To do this, since we have shown that the  $L \rightarrow \Gamma$  and  $\Gamma \rightarrow L$  rates are dependent [cf. Eq. (7)], we vary both  $\gamma_{\Gamma L}$  and  $\gamma_{L\Gamma}$  but keep the ratio  $R$  constant. The solid line corresponds to the experimental data<sup>5</sup> and the dashed line the original fit. For the dash-dotted line,  $\gamma_{\Gamma L}$  and  $\gamma_{L\Gamma}$  are increased by a factor of 5, whereas for the dotted line, they are decreased by a factor of 5. As can be seen, the rise time is not strongly affected when the rate is increased, again consistent with Eq. (19), provided the ratio remains constant. When the rate is divided by a factor of 5, however, then one is no longer in the limit  $\gamma_{\Gamma L} \gg \gamma_{\Delta}$  and a slight change in the time-dependent mobility is observed at short times. For slow intervalley scattering, i.e.,  $0.2 \times \gamma_{\Gamma L}$ , there is not a rapid transfer of the initial electron populations into the  $L$  valleys as in the other cases. If the  $\Gamma \rightarrow L$  intervalley rate were this slow, one should see these effects in the experimental data. The fact that they are not seen shows that the  $\Gamma \rightarrow L$  rate cannot be this slow and indicates that the intervalley rate  $\gamma_{\Gamma L}$  is greater than the POP scattering rate  $\gamma_{\Delta}$ .

In Fig. 6, we show the sensitivity of the rise time of the mobility to the density of states ratio  $R$ . The solid line is the experimental data and the dashed line is from the original calculated results. In all cases, we hold  $\gamma_{\Gamma L}$  constant and vary  $\gamma_{L\Gamma}$  to change the ratio  $R$ . For the dash-dotted line, the ratio is doubled, whereas for the dotted line it is halved. We can see that the data are very sensi-

tive to this ratio. In fact, the curves are similar to those in Fig. 4, which we should expect based on Eq. (19).

These results show that the  $\Gamma \rightarrow L$  intervalley rate is faster than the POP rate. This agrees with the transient nonlinear absorption experiments of Rosker, Wise, and Tang,<sup>7</sup> Schoenlein *et al.*,<sup>8</sup> and Becker *et al.*,<sup>9,10</sup> which predict fast  $\Gamma \rightarrow L$  rates. Also, even though the  $L \rightarrow \Gamma$  rate is slower than the POP rate, the return time of carriers from the  $L$  valley is still limited by the relaxation of the electrons in the  $\Gamma$  valley.

#### FOUR-STATE MODEL

The three-state model is useful for determining the  $\Gamma$ - and  $L$ -valley populations and is applicable for describing experiments which depend only on which valley the electrons occupy. Other experiments, such as the rise time of the band-edge photoluminescence, are more sensitive to the state within the  $\Gamma$  valley that the electrons occupy. In particular, the photoluminescence experiments require that the electrons be at the bottom of the conduction band to contribute. Therefore the three-state model is not applicable. To account for this additional structure, we propose the four-state model shown schematically in Fig. 7. In the four-state model, an additional state is added in the  $\Gamma$  valley representing electrons at the band edge and is labeled  $\Gamma_{BE}$ . The  $\Gamma^<$  state now represents all the electrons with energies ranging from one optic phonon energy above the band edge to energies just below the threshold for scattering to the  $L$  valley. For an electron to scatter from the top of the  $\Gamma^<$  state to the bottom of the  $\Gamma$  valley into the  $\Gamma_{BE}$  state, requires that the electron emit approximately eight optical phonons (the first seven emissions keep the electron within the  $\Gamma^<$  state). The scattering rate from  $\Gamma^<$  to  $\Gamma_{BE}$ , denoted by  $\gamma_{BE}$ , is therefore approximately  $\gamma_{\Delta}/8$ .

In matrix form, the four-state model is given as

$$\frac{d}{dt} \begin{bmatrix} n_{\Gamma^>} \\ n_L \\ n_{\Gamma^<} \\ n_{\Gamma_{BE}} \end{bmatrix} = \begin{bmatrix} -(\gamma_{\Gamma L} + \gamma_{\Delta}) & \gamma_{L\Gamma} & 0 & 0 \\ \gamma_{\Gamma L} & -\gamma_{L\Gamma} & 0 & 0 \\ \gamma_{\Delta} & 0 & -\gamma_{BE} & 0 \\ 0 & 0 & \gamma_{BE} & 0 \end{bmatrix} \begin{bmatrix} n_{\Gamma^>} \\ n_L \\ n_{\Gamma^<} \\ n_{\Gamma_{BE}} \end{bmatrix} \quad (23)$$

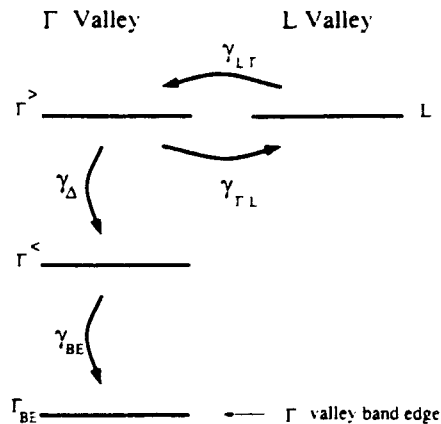


FIG. 7. The four-state model. Here  $\Gamma^>$  represents electrons in the  $\Gamma$  valley that are energetically able to transfer to the  $L$ -valley state.  $\Gamma^<$  includes all electrons in the  $\Gamma$  valley that are just below the energy threshold for transfer to the  $L$  valley to those electrons that are just above the band edge.  $\Gamma_{BE}$  represents the electrons in the  $\Gamma$  valley at the band edge. Band-edge photoluminescence is sensitive to the number of electrons in the  $\Gamma_{BE}$  state. Scattering from  $\Gamma^<$  to  $\Gamma_{BE}$  involves the emission of several phonons (approximately 8 in GaAs) for electrons to go from just below the threshold for intervalley transfer to the bottom of the band edge, and the rate is given by  $\gamma_{BE}$ .

The eigenvalues for this matrix are easily found by expanding the determinant by cofactors of the last column. They are 0,  $\lambda_+$ ,  $\lambda_-$ , and  $-\gamma_{BE}$ .

One can solve Eq. (23) by noting that the coupled equations for  $n_{\Gamma^>}$  and  $n_L$  are the same as before, and that the expression for  $n_{\Gamma^<}$  can be found by using an integrating factor and directly integrating the previous expressions. The expression for  $n_{\Gamma_{BE}}$  can then be found by integrating the expression for  $n_{\Gamma^<}$ ,

$$n_{\Gamma^<}(t) = \gamma_{\Delta} \int_0^t dt' e^{-\gamma_{BE}(t-t')} n_{\Gamma^>}(t'), \quad (24)$$

$$n_{\Gamma_{BE}}(t) = \gamma_{BE} \int_0^t dt' n_{\Gamma^<}(t').$$

From these equations, one obtains the solutions

$$n_{\Gamma^<}(t) = \frac{n_{\Gamma^>}^0 \gamma_{\Delta}}{\lambda_- - \lambda_+} \left[ \left( \frac{\gamma_{L\Gamma} + \lambda_+}{\lambda_- + \gamma_{BE}} \right) (e^{\lambda_+ t} - e^{-\gamma_{BE} t}) - \left( \frac{\gamma_{L\Gamma} + \lambda_-}{\lambda_- + \gamma_{BE}} \right) (e^{\lambda_- t} - e^{-\gamma_{BE} t}) \right], \quad (25)$$

$$n_{\Gamma_{BE}}(t) = \frac{n_{\Gamma^>}^0 \gamma_{\Delta} \gamma_{BE}}{\lambda_- - \lambda_+} \left[ \left( \frac{\gamma_{L\Gamma} + \lambda_+}{\lambda_- + \gamma_{BE}} \right) \left[ \frac{(e^{\lambda_+ t} - 1)}{\lambda_+} + \frac{(e^{-\gamma_{BE} t} - 1)}{\gamma_{BE}} \right] - \left( \frac{\gamma_{L\Gamma} + \lambda_-}{\lambda_- + \gamma_{BE}} \right) \left[ \frac{(e^{\lambda_- t} - 1)}{\lambda_-} + \frac{(e^{-\gamma_{BE} t} - 1)}{\gamma_{BE}} \right] \right]. \quad (26)$$

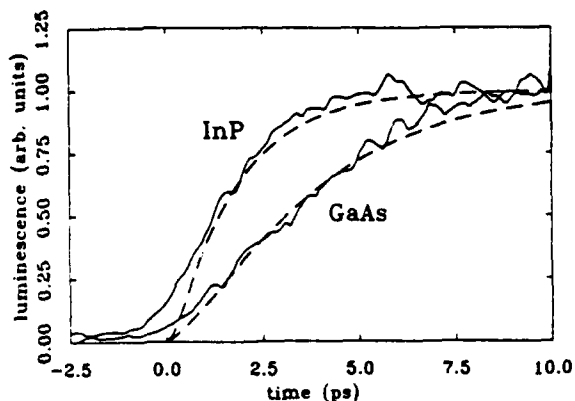


FIG. 8. Rise time for the luminescence in GaAs and InP as calculated from the four-state model. The solid lines are from the experimental work of Shah *et al.* (Ref. 2). The dashed lines are the results of the four-state model. For InP, the intervalley scattering rates  $\gamma_{rL}$  and  $\gamma_{Lr}$  are set to zero keeping all other rates the same. As can be seen, the rate-equation model accurately predicts the observed differences between GaAs and InP. Differences between the experimental curves and rate-equation model at short times originate from the finite temporal width of the laser pulse not accounted for in the four-state model.

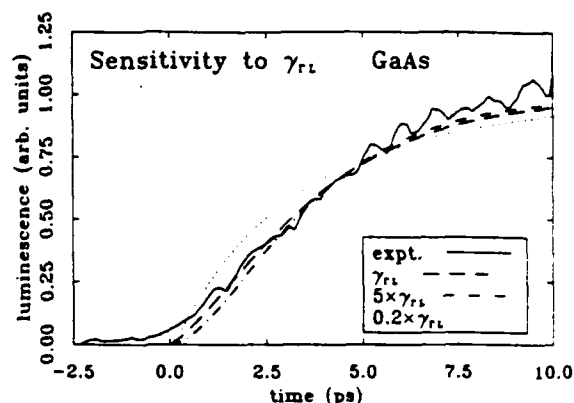


FIG. 10. Sensitivity of the rise time of the luminescence in GaAs to the intervalley scattering rate. The solid line is the experimental curve of Shah *et al.* (Ref. 2), and the dashed line the result of the four-state model. For the dash-dotted and dotted lines, the intervalley scattering rates are changed so that the ratio  $R$  remains constant. For the dash-dotted line the rate is increased by a factor of 5, while for the dotted line, the rate is divided by a factor of 5. As can be seen from the figures, the rise time of the luminescence is insensitive to the intervalley rates provided the ratio of the equilibrium populations is constant.

Results for the four-state model are shown in Figs. 8–12. The experimental luminescence is proportional to the density of electrons at the bottom of the band, i.e., the population of  $\Gamma_{BE}$ . In Fig. 8, we show the experimental data for the rise time of the luminescence in GaAs and InP from Shah *et al.*<sup>2</sup> (solid lines). We also plot the results of the four-state model (dashed lines). We use a  $\gamma_{BE}$  rate of  $6 \times 10^{11} \text{ s}^{-1}$ , approximately  $\frac{1}{3}$  of  $\gamma_{\Delta}$ . For InP, since the  $L$  valleys lie too high in energy for intervalley transfer in the Shah *et al.* experiment,<sup>2</sup> we set the intervalley rates to zero keeping all other rates the same. As can be seen from the curves, the rate-equation model ac-

curately predicts the dependence of the rise time of the luminescence for both InP and GaAs. Since the total number of electrons in the  $\Gamma$  valley as a function of time does not change between the three-state and four-state models (only the occupation of the different  $\Gamma$  valley states changes), the rise time of the mobility is exactly the same as before.

In Fig. 9, we check the sensitivity of the luminescence rise time to the POP scattering rate. The solid line is from the experiment,<sup>2</sup> the dashed is from the original fit, and the dash-dotted and dotted correspond to doubling and halving the POP rate, respectively. Just as for the

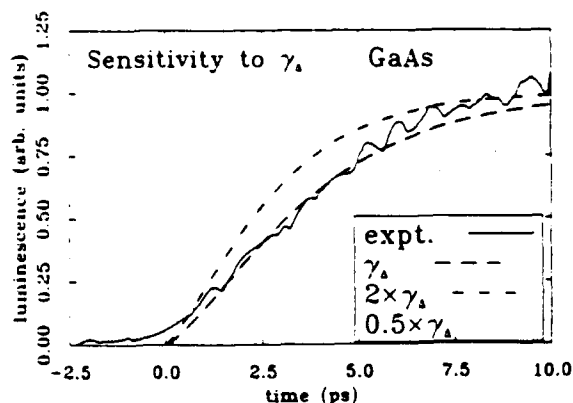


FIG. 9. Sensitivity of the rise time of the luminescence for GaAs in the four-state model to the electron-phonon scattering rate ( $\gamma_{\Delta}$ ). The solid line is the experimental data of Shah *et al.* (Ref. 2) and the dashed line is the result of the four-state model. For the dash-dotted line, the electron-phonon scattering rate is doubled, while for the dotted line, the rate is halved. As can be seen, the rise time of the luminescence is very sensitive to this rate.

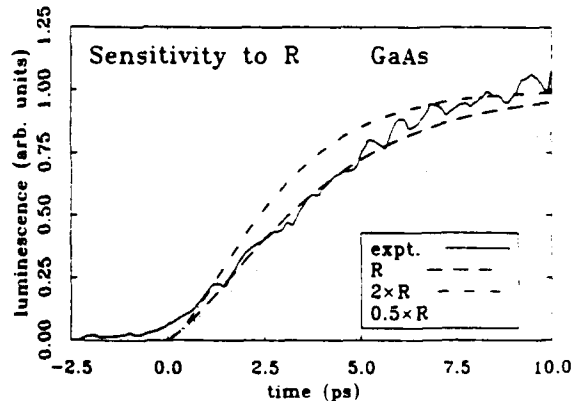


FIG. 11. Sensitivity of the rise time of the luminescence in GaAs to the density of state ratio  $R$ . The solid line is the experimental work of Shah *et al.* (Ref. 2) and the dashed line the solution to the four-state model. For the dash-dotted line, the ratio of the populations is doubled, while for the dotted line, it is cut in half. The curves are similar to those in Fig. 9, showing that the rise time of the luminescence depends on the rate  $\gamma_{\Delta}$  (as well as  $\gamma_{BE}$ ).

mobility, we see that the rise time of the luminescence is very sensitive to this rate. The net transfer of carriers from the  $L$  to the  $\Gamma$  valley depends strongly on the POP scattering rate within the  $\Gamma$  valley.

In Fig. 10, we show the sensitivity of the luminescence to the intervalley scattering rates keeping the ratio  $R$  constant. As before, there is not a strong dependence on the magnitude of the rate, even when divided by a factor of 5, provided the ratio is kept constant. We thus see that experiments measuring the rise time of the luminescence are insensitive to the intervalley rates, and only depend on the density of states in the two valleys and the inelastic scattering rate within the  $\Gamma$  valley.

In Fig. 11, we show the sensitivity to the ratio  $R$ . Again, the luminescence is sensitive to this ratio as predicted by Eq. (19).

### CONCLUSIONS

We have provided and solved a set of rate equations for intervalley scattering in compound semiconductors such as GaAs or InP. Using standard values for the transport parameters, solutions to these rate-equation models predict the experimental trends in time-dependent mobility and luminescence experiments quite well. Although these rate equations are simpler than full Monte Carlo modeling<sup>17,18</sup> or numerical solutions to the Boltzmann equation,<sup>25</sup> they nonetheless illustrate several key points.

(i) The  $\Gamma \rightarrow L$  and the  $L \rightarrow \Gamma$  intervalley scattering rates are *dependent* and related, through detailed balance, to the densities of states in each valley.

(ii) In time-dependent mobility and time-resolved photoluminescence experiments, one measures the *depopulation rate* of the  $L$  valley. The depopulation rate of the  $L$  valleys is *not* the same as the  $L \rightarrow \Gamma$  intervalley scattering rate unless the inelastic-scattering rate in the  $\Gamma$  valley is significantly larger than the  $\Gamma \rightarrow L$  rate. From an estimate of the transport parameters that are applicable to GaAs and InP, we find excellent agreement between the

rate equations and experimental data for both the time-dependent mobility and the rise time of the luminescence. The scattering rates suggest that the  $L$ -valley depopulation is dominated by the energy relaxation of the electrons in the  $\Gamma$  valley. That is, POP scattering in the  $\Gamma$  valley acts as the bottleneck for the return of the electrons from the  $L$  valley. This return is not limited by the  $L \rightarrow \Gamma$  intervalley scattering rate. This suggests that time dependent mobility and band-edge luminescence experiments are not optimum for determining the intervalley scattering rates.

(iii) The initial low mobility in the NAC experiment can only be explained by a rapid transfer of electrons from their photoexcited states into the  $L$  valleys, suggesting a fast  $\Gamma \rightarrow L$  rate. This is consistent with the insensitivity of the rise time of the luminescence in GaAs to the  $\Gamma \rightarrow L$  rate, as well as the transient nonlinear absorption experiments of Rosker, Wise, and Tang,<sup>7</sup> Schoenlein *et al.*,<sup>8</sup> and Becker *et al.*,<sup>9,10</sup> which predict fast  $\Gamma \rightarrow L$  rates. Thus this is further evidence that the  $\Gamma \rightarrow L$  intervalley scattering rate is *faster* than the POP scattering rate.

While the rate equation models are simple, they nonetheless provide valuable insight into the qualitative carrier dynamics in compound semiconductors and isolate characteristics often lost in more detailed calculations.

### ACKNOWLEDGMENTS

We are thankful to Frank Wise and Pradeep Kumar for useful discussions during this work. We are also grateful for the hospitality of the Institute for Theoretical Physics where part of this work was completed. This work was supported in part by the National Science Foundation through Grants Nos. DMR8957382 and PHY89-04035 and by the U.S. Office of Naval Research through Grant No. N00091-J-1956.

<sup>1</sup>S. M. Sze, *Physics of Semiconductor Devices*, 2nd ed. (Wiley, New York, 1981), Chap. 11.

<sup>2</sup>J. Shah, B. Deveaud, T. C. Damen, W. T. Tsang, A. C. Gosard, and P. Lugli, *Phys. Rev. Lett.* **59**, 222 (1987).

<sup>3</sup>T. Elsaesser, J. Shah, L. Rota, and P. Lugli, *Phys. Rev. Lett.* **66**, 1757 (1991).

<sup>4</sup>W. B. Wang, N. Ockman, M. A. Cavicchia, and R. R. Alfano, *Appl. Phys. Lett.* **57**, 395 (1990).

<sup>5</sup>M. C. Nuss, D. H. Auston, and F. Capasso, *Phys. Rev. Lett.* **58**, 2355 (1987).

<sup>6</sup>C. L. Tang, I. A. Walmsley, and F. W. Wise, *Appl. Phys. Lett.* **52**, 850 (1988).

<sup>7</sup>M. Rosker, F. Wise, and C. L. Tang, *Appl. Phys. Lett.* **49**, 1726 (1986).

<sup>8</sup>R. W. Schoenlein, W. Z. Lin, S. D. Brorson, E. P. Ippen, and J. G. Fujimoto, *Appl. Phys. Lett.* **51**, 1442 (1987).

<sup>9</sup>P. C. Becker, H. L. Fragnito, C. H. Brito Cruz, J. Shah, R. L. Fork, J. E. Cunningham, J. E. Henry, and C. V. Shank, *Appl.*

*Phys. Lett.* **53**, 2089 (1988).

<sup>10</sup>P. C. Becker, H. L. Fragnito, C. H. Brito Cruz, R. L. Fork, J. E. Cunningham, J. E. Henry, and C. V. Shank, *Phys. Rev. Lett.* **61**, 1647 (1988).

<sup>11</sup>B. P. Zakharchenya, D. N. Mirlin, V. I. Perel, and I. I. Reshina, *Usp. Fiz. Nauk.* **136**, 459 (1982) [*Sov. Phys. Usp.* **25**, 143 (1982)].

<sup>12</sup>G. Fasol, W. Hackenberg, H. P. Hughes, K. Ploog, E. Bauser, and H. Kano, *Phys. Rev. B* **41**, 1461 (1990).

<sup>13</sup>R. G. Ulbrich, J. A. Kash, and J. C. Tsang, *Phys. Rev. Lett.* **62**, 949 (1989).

<sup>14</sup>C. J. Stanton, Ph.D. thesis, Cornell University, 1986.

<sup>15</sup>K. Hess, *Advanced Theory of Semiconductor Devices* (Prentice-Hall, Englewood Cliffs, NJ, 1988).

<sup>16</sup>F. H. Pollak, C. W. Higginbotham, and M. Cardona, *J. Phys. Soc. Jpn. Suppl.* **21**, 20 (1966).

<sup>17</sup>C. J. Stanton, D. W. Bailey, and K. Hess, *Phys. Rev. Lett.* **65**, 231 (1990).



- <sup>18</sup>D. W. Bailey, C. J. Stanton, and K. Hess, Phys. Rev. B **42**, 3423 (1990).
- <sup>19</sup>E. M. Conwell, in *Solid State Physics, Advances in Research and Applications*, edited by F. Seitz, D. Turnbull, and H. Ehrenreich (Academic, New York, 1967), Vol. 9.
- <sup>20</sup>L. Reggiani, in *Hot-Electron Transport in Semiconductors*, edited by L. Reggiani (Springer-Verlag, Berlin, 1985), Chap.

2.

- <sup>21</sup>D. W. Bailey *et al.*, Solid-State Electron. **31**, 467 (1988).
- <sup>22</sup>M. J. Kann, A. M. Krizan, and D. K. Ferry, Solid-State Electron. **32**, 1831 (1989).
- <sup>23</sup>H. Shichijo and K. Hess, Phys. Rev. B **23**, 4197 (1981).
- <sup>24</sup>H. Shichijo, Ph.D. thesis, University of Illinois, 1980.
- <sup>25</sup>Y. S. Sun and C. J. Stanton, Phys. Rev. B **43**, 2285 (1991).

time-  
ence.  
pula-  
elec-  
he  $\Gamma$   
elec-  
y the  
time  
peri-  
alley

ment  
trons  
gest-  
sensi-  
o the  
ption  
nlein  
 $\gamma \rightarrow L$   
inter-  
ering

they  
ative  
i iso-  
cula-

umar  
also  
etical  
This  
ience  
and  
earch

ork, J.  
Rev.

Reshi-  
5, 143

ausen,

. Lett.

Devices

Phys.

tt. 65.

## **Studies of Intervalley Scattering using Tunable Femtosecond Pulses**

**M. Ulman, L. H. Acioli, C. J. Stanton<sup>†</sup>, E. P. Ippen, and J. G. Fujimoto**

**Department of Electrical Engineering and Computer Science  
Research Laboratory of Electronics  
Massachusetts Institute of Technology  
Cambridge, MA 02139  
(617) 253-8528**

**<sup>†</sup>Department of Physics  
University of Florida  
Gainesville, FL 32611**

### **Abstract**

We report experimental and theoretical investigations of intervalley scattering in Al-GaAs. Femtosecond absorption saturation measurements are performed using tunable 50 fs pulses and results interpreted using an ensemble Monte Carlo simulation as well as a rate equation model.

## **Studies of Intervalley Scattering using Tunable Femtosecond Pulses**

**M. Ulman, L. H. Acioli\*, C. J. Stanton<sup>†</sup>,  
E. P. Ippen, and J. G. Fujimoto**

**Department of Electrical Engineering and Computer Science  
Research Laboratory of Electronics  
Massachusetts Institute of Technology  
Cambridge, MA 02139  
(617) 253-8528**

**<sup>†</sup>Department of Physics  
University of Florida  
Gainesville, FL 32611**

### **Summary**

Intervalley scattering in AlGaAs has been studied by a variety of techniques. Subpicosecond and CW luminescence spectroscopy<sup>[1,2]</sup> and femtosecond absorption saturation<sup>[3,4]</sup> measurements have been used in attempts to determine the intervalley scattering rates and deformation potentials. While these measurements were the first to set limits on the intervalley scattering rates, they do not directly measure the intervalley scattering from the initial optically excited states and discrepancies exist between reported values. Most of these investigations measure the return of carriers from the satellite valleys by probing the occupancy of the  $\Gamma$  valley at energies near the conduction band edge. These measurements are strongly affected by inelastic scattering within the  $\Gamma$  valley<sup>[5]</sup>.

We report investigations of intervalley scattering in AlGaAs using tunable femtosecond pulses. By systematically varying the wavelength and spectral content of the pulses, different scattering channels may be isolated, such as scattering to the  $L$  satellite valley.

Pump probe absorption saturation measurement permits a direct investigation of scattering from the initial optically prepared carrier distributions and allows a sensitive and direct measurement of intervalley scattering processes.

The laser source in our experiments is a dispersion compensated colliding pulse mode-locked ring dye laser (CPM). 40 fs pulses from the CPM are amplified in a high repetition rate copper vapor laser pumped dye amplifier. The amplified pulses are focussed on a jet of ethylene glycol to generate a femtosecond white light continuum. The continuum is filtered in the frequency domain with a grating Fourier filter<sup>[6]</sup> shown schematically in figure 1. This filter allows continuous control of both the center wavelength and bandwidth or duration of the femtosecond pulses. In addition, arbitrary temporal pulse trains may be generated by appropriate masking in the Fourier plane. Femtosecond transient absorption saturation is measured using pump-probe techniques with differential detection. Experiments are performed using antireflection coated 0.2 micron thick MBE samples of  $\text{Al}_x\text{Ga}_{1-x}\text{As}$  which are clad by  $\text{Al}_{0.6}\text{Ga}_{0.4}\text{As}$ .

The mole fraction of Al can be explicitly chosen to vary the band structure and select desired transitions. For example, in  $\text{Al}_{0.1}\text{Ga}_{0.9}\text{As}$ , scattering to the *L* valley is energetically allowed for carriers photoexcited at energies of  $\sim 1.8$  eV or greater (see Fig. 2). The use of frequency synthesis techniques for these measurements represents a powerful approach since the wavelength, pulse duration and the initial spectral distribution of carriers can be systematically controlled. This permits a comprehensive investigation of carrier dynamics. For example, figure 3 shows pump probe measurements of transient absorption saturation behavior in  $\text{Al}_{0.1}\text{Ga}_{0.9}\text{As}$  at 1.86 eV and at 1.72 eV using 50 fs pulses. The presence or absence of the intervalley scattering channel to the *L* valley is manifest as a change in the behavior of the initial femtosecond transient in the data. Systematic measurements may be performed as a function of both photon energy and wavelength.

The determination of fundamental scattering parameters directly from pump probe data is complicated by the fact that several scattering processes and transitions are involved. Thus we use two theoretical approaches to interpret our data. The first technique

is based on a discretization of the Boltzman transport equation and the scattering states which yields a simple rate equation model. This describes the carrier populations in the  $L$  valley, high in the  $\Gamma$  valley, and at the band edge<sup>[5]</sup>. This model represents a compact and simple calculational approach which qualitatively predicts the effects of different carrier-carrier and intervalley scattering rates on the experimental results. However, in order to obtain a more comprehensive understanding of the carrier dynamics we have developed a full ensemble Monte Carlo simulation of the carrier dynamics. 40,000 electrons and holes are simulated and scattering mechanisms included are electron - polar optic phonon, electron - electron with time dependent screening, electron - intervalley, hole - non-polar optical phonon, and hole - hole. The distribution functions generated by the Monte Carlo simulation are used to predict differential transmission curves which may be compared directly to the experimental data. Monte Carlo techniques represent a rigorous approach for studying carrier dynamics since different experimental parameters can be used as inputs for the simulations. In addition, the effects of different scattering processes may be studied independently by isolating them in the simulation.

We gratefully acknowledge C.A. Wang from M.I.T. Lincoln Laboratory for preparing the MBE samples used in this investigation. \*LHA's permanent address is Dept. de Fisica, Univ. Fed. de Pernambuco, Brazil.

## References

- [1] J. Shah, B. Deveaud, T. C. Damen, W. T. Tsang, A. C. Gossard, and P. Lugli, *Phys. Rev. Lett.* **59**, 2222 (1987).
- [2] R. G. Ulbrich, J. A. Kash, and J. C. Tsang, *Phys. Rev. Lett.* **62**, 949 (1989).
- [3] M. C. Nuss, D. H. Auston, and F. Capasso, *Phys. Rev. Lett.* **58**, 2355 (1987).
- [4] J. Y. Bigot, M. T. Portella, R. W. Schoenlein, J. E. Cunningham, and C. V. Shank, *Phys. Rev. Lett.* **65**, 3429 (1990); P. C. Becker, H. L. Fragnito, C. H. Brito Cruz,

J. Shah, R. L. Fork, J. E. Cunningham, J. E. Henry, and C. V. Shank, *Appl. Phys. Lett.* **53**, 2089 (1988).

[5] C. J. Stanton and D. W. Bailey, "Rate Equations for the Study of Femtosecond Intervalley Scattering in Compound Semiconductors," submitted for publication.

[6] A. M. Weiner, J. P. Heritage, and E. M. Kirschner, *J. Opt. Soc. Am. B* **5**, 1563 (1988).

**Figure Captions**

**Figure 1.** Schematic diagram of the experimental apparatus. A grating Fourier filter is used to control wavelength and bandwidth.

**Figure 2.** Schematic bandstructure of  $\text{Al}_{0.1}\text{Ga}_{0.9}\text{As}$  showing optical transitions above and below the L valley.

**Figure 3.** Transient absorption saturation data for pump-probe energies above (1.86 eV) and below (1.72 eV) the L satellite valley. The photoexcited carrier density is  $\sim 10^{18} \text{ cm}^{-3}$ .

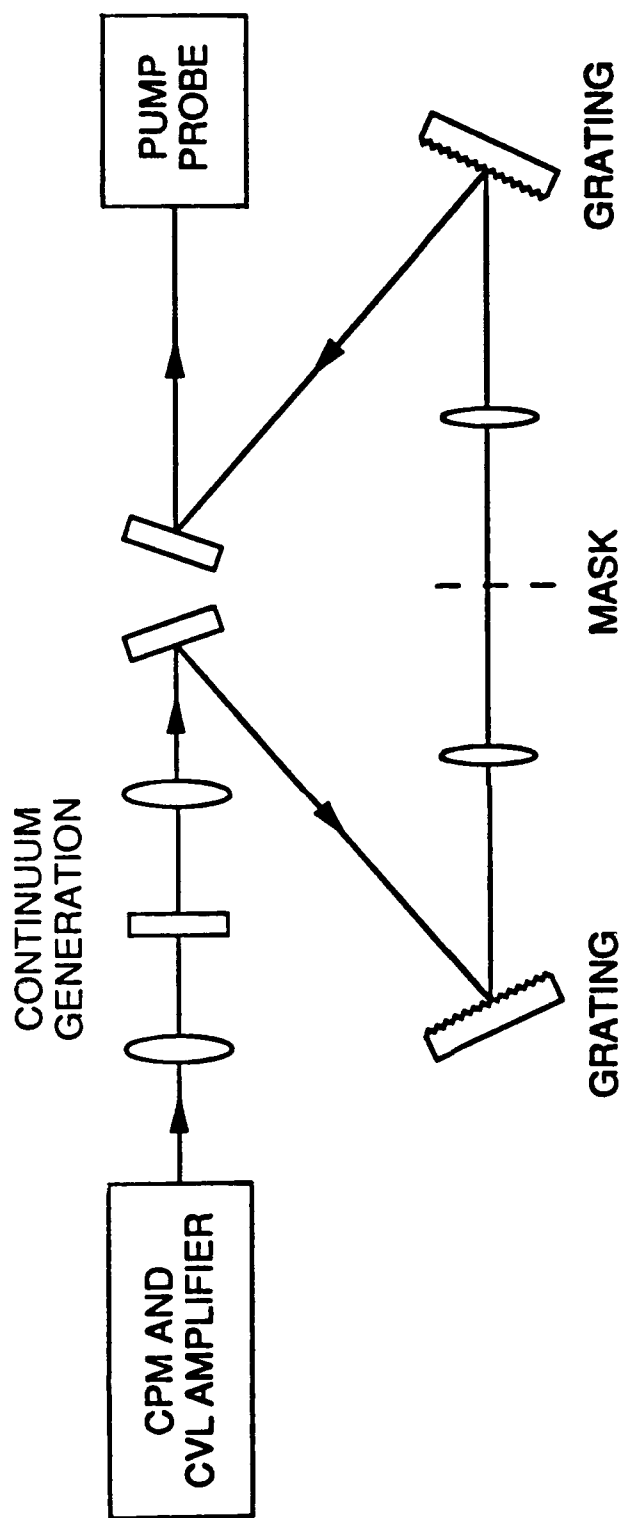


## Figure 1



# $\text{Al}_{0.1}\text{Ga}_{0.9}\text{As}$

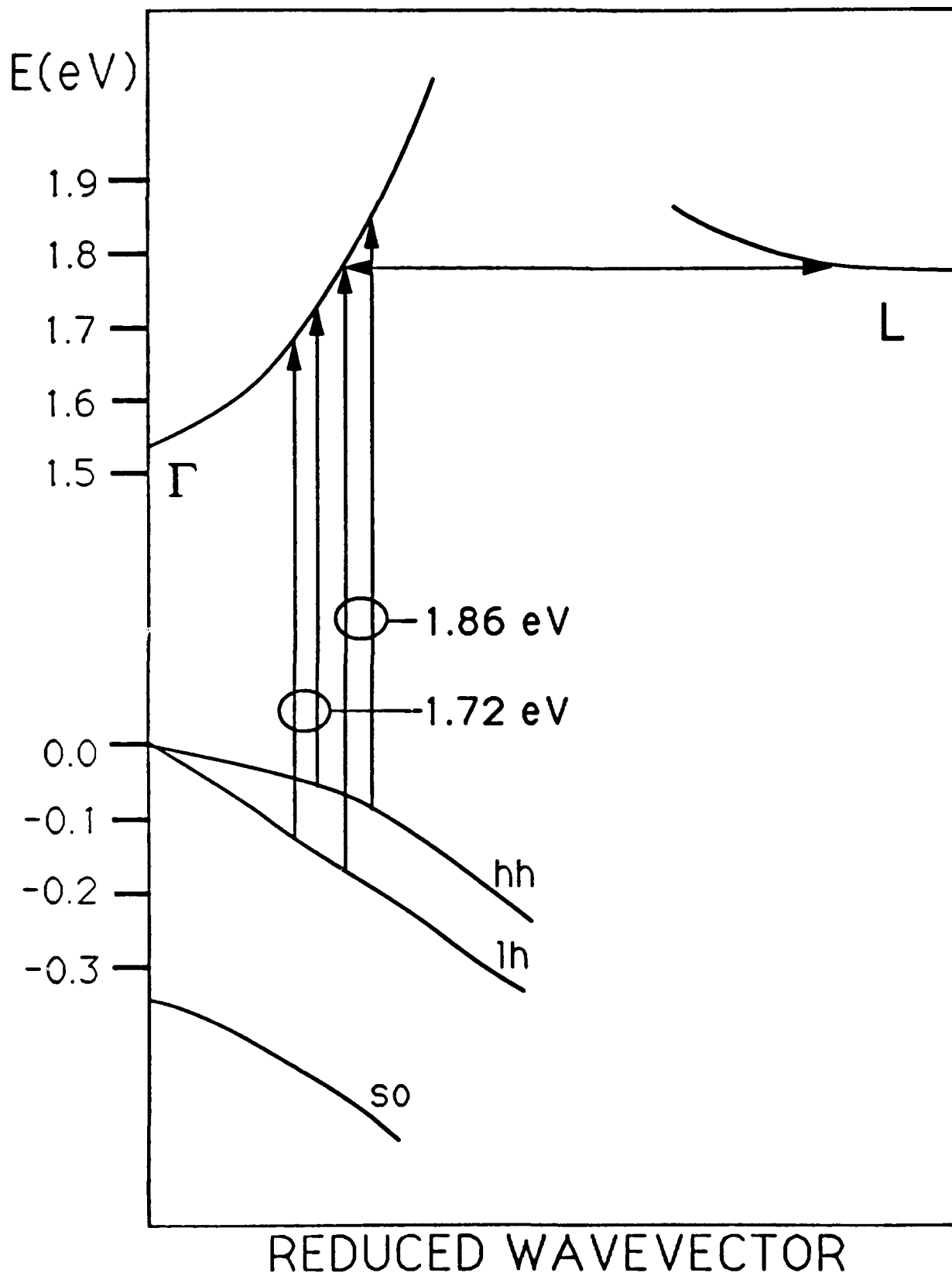


Figure 2

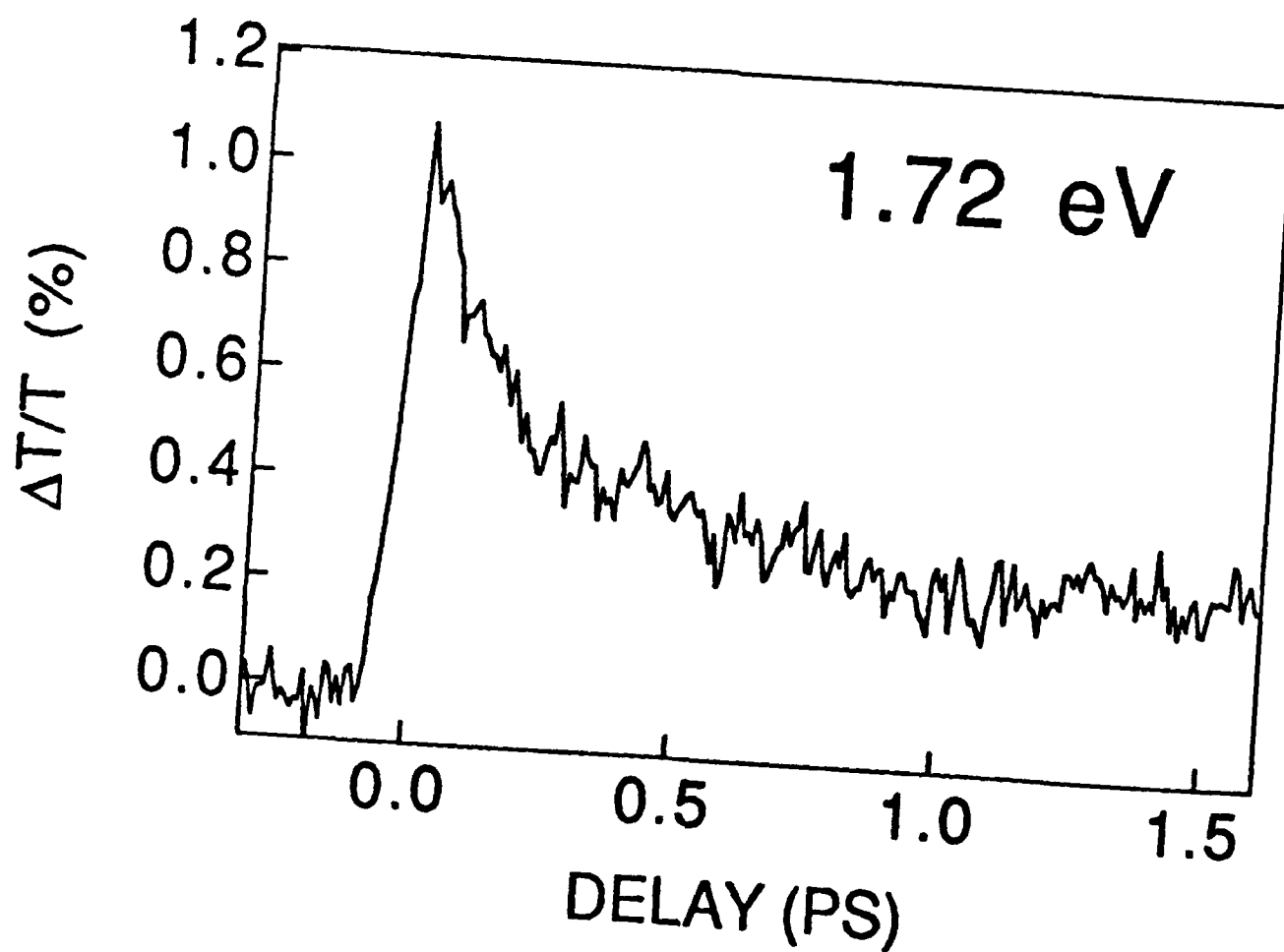
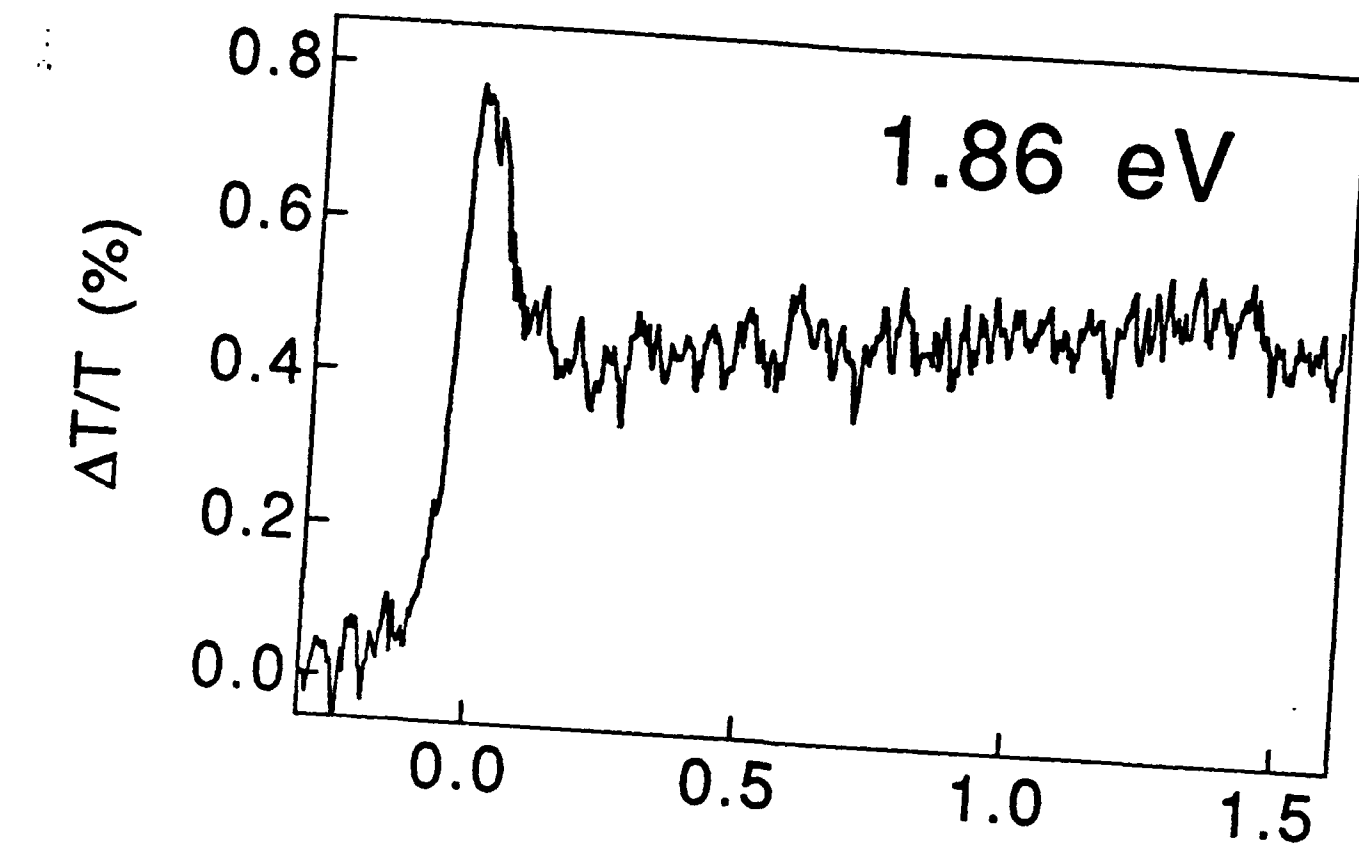


Figure 3

Abstract Submitted  
for the March 1989 Meeting of the  
American Physical Society  
November 20, 1991

Sorting Category 15B

**Theory of Optical Gain in Silicon Quantum Wire Lasers.** G. D. SANDERS, C. J. STANTON, *University of Florida*;<sup>\*</sup> Y. C. CHANG, *University of Illinois at Urbana-Champaign* - We present theoretical calculations of gain, refractive index change, and differential gain for lasers made from regular arrays of silicon wires. We use a second-nearest-neighbor empirical tight-binding model to calculate subband energies and optical matrix elements. Laser properties are studied in a density matrix formalism with intrasubband relaxation. For narrow quantum wires, the silicon wire band gap is direct and the oscillator strength for interband transitions are comparable to that of direct gap materials such as bulk GaAs. Thus the enhanced optical matrix elements combined with an enhanced density of states leads to large optical gain. We find laser performance is sensitive to wire size and polarization.

<sup>\*</sup>Supported by the National Science Foundation through Grant No. DMR8957382 and by the U.S. Office of Naval Research through Grant No. N00091-J-1956.



C. J. Stanton  
Physics Department  
University of Florida  
215 Williamson Hall  
Gainesville, FL 32603  
(phone: 904 392-8753)  
(email: stanton@laguna.phys.ufl.edu)

Prefer Standard Session

Abstract Submitted  
for the March 1992 Meeting of the  
American Physical Society  
16-20 March 1992

Sorting Category 24b

**Rate Equations for the Study of Intervalley Scattering in Compound Semiconductors** C. J. Stanton, *University of Florida*,\* and D. W. Bailey, *University of South Carolina* - We present solutions to a set of rate equations for the electron dynamics after photoexcitation by a 2.0 eV laser in GaAs and InP. Results obtained, although simpler than full Monte Carlo solutions, closely follow the experimental data and provide insight into intervalley scattering. Calculations shows that the net return time of electrons from the satellite L valleys into the  $\Gamma$  valley is not limited by the intervalley scattering rate, but is instead limited by polar optic phonon scattering rate within the  $\Gamma$  valley. This shows that the time dependent mobility and luminescence experiments depend on the *L* valley depopulation rate, which differs from the  $L \rightarrow \Gamma$  intervalley scattering rate. Results further suggest that the  $\Gamma \rightarrow L$  scattering rate is faster than the polar optic phonon scattering rate.

\* Supported by the ONR through grant # N00091-J-1956.



C. J. Stanton  
Department of Physics  
University of Florida  
Williamson Hall  
Gainesville, FL 32611  
(phone: 904-392-8753)

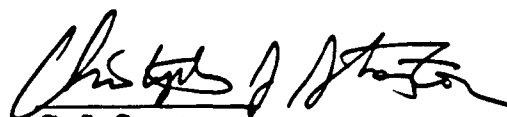
Prefer Standard Session

Abstract Submitted  
for the March 1992 Meeting of the  
American Physical Society  
16-20 March 1992

Sorting Category 24b

**Tunable Pump-Probe Nonlinear Absorption Spectroscopy in AlGaAs** D. W. Bailey, *University of South Carolina*; C. J. Stanton, *University of Florida*;\* M. Ulman, L. H. Acioli, J. G. Fujimoto, *MIT*; \* - We report the results of experiments and calculations of the nonlinear transient absorption in AlGaAs systems. In the experiments, the wavelength of the pump and probe pulses can be simultaneously varied from 500 nm to 800 nm. This, for the first time, allows one to selectively study intervalley scattering, since one can tune the region of photoexcited electrons above and below the threshold for scattering into the satellite L valleys. Theoretical calculations based on ensemble Monte Carlo simulations, matrix method techniques and rate equations allow one to decipher the effects of 1) intervalley scattering; 2) density dependence and carrier-carrier scattering; 3) polar optic phonon scattering. Results show these tunable pump-probe experiments are more sensitive and better suited to determining intervalley scattering rates than previous time-dependent mobility and band edge luminescence experiments.

\* Supported by the ONR through grant # N00091-J-1956.



C. J. Stanton  
Department of Physics  
University of Florida  
Williamson Hall  
Gainesville, FL 32611  
(phone: 904-392-8753)

Prefer Standard Session

ATTACHMENT NUMBER 3REPORTS AND REPORTS DISTRIBUTIONREPORT TYPES

- (a) Performance (Technical) Report(s) (Include letter report(s))  
Frequency: Annual
- (b) Final Technical Report, issued at completion of Grant.
- (c) Final Financial Status Report (SF 269)

REPORTS DISTRIBUTION

<u>ADDRESSEES</u>	<u>REPORT TYPES</u>	<u>NUMBER OF COPIES</u>
Scientific Officer Code: 1114SS Larry R. Cooper Office of Naval Research 800 North Quincy Street Arlington, Virginia 22217-5000	(a) & (b)	3
Administrative Grants Officer Office of Naval Research Resident Representative N66017 Administrative Contracting Officer Massachusetts Institute of Tech. Room E19-628 Cambridge, MA 02139-4309	(a) & (b) & (c)	1
Director, Naval Research Laboratory Attn: Code 2627 Washington, DC 20375	(a) & (b)	1
Defense Technical Information Center Building 5, Cameron Station Alexandria, Virginia 22304-6145	(a) & (b)	2
DoD - Washington Headquarters Services Installation Accounting Branch Rm. #3B269, The Pentagon Washington, D.C. 20301--1155	(a), (b), & (c)	2
Office of Civil Applications OSD/SDIO/CA Washington, D.C. 20301-7100	(a) (b) & (c)	2

If the Scientific Officer directs, the Grantee shall make additional distribution of technical reports in accordance with a supplemental distribution list provided by the Scientific Officer. The supplemental distribution list shall not exceed 250 addresses.